Blue light toxicity drives the gut microbiota-mediated lipid accumulation in *Drosophila*

Authors

Yuta Takada[1], Toshiharu Ichinose[2,3], Naoyuki Fuse[4], Kokoro Saito[3], Wakako Ikeda-Ohtsubo[1], Hiromu Tanimoto[3], Masatoshi Hori[1]

Affiliations

[1]Graduate School of Agricultural Sciences, Tohoku University, Japan

[2]Frontier Research Institute for Interdisciplinary Sciences, Tohoku University, Japan

[3]Graduate School of Life Sciences, Tohoku University, Japan

[4]Graduate School of Pharmaceutical Sciences, Tohoku University, Japan

Corresponding to Yuta Takada or Masatoshi Hori

yutatakada38@gmail.com

masatoshi.hori.a3@tohoku.ac.jp

Abstract

Blue light (BL), abundant in sunlight, is highly toxic to many insect species when exposure is excessive. While the physiological mechanisms of BL toxicity are being revealed, the evolutionary responses remain less explored. In this study, using *Drosophila melanogaster* as a model system, we conducted laboratory selection for over 60 generations under excessive BL exposure. The selected line (SL) flies exhibited enhanced BL-tolerance, and also increased body weight and lipid accumulation. Interestingly, we found elongated midgut in the SL flies, and increased microbiota, which was dominated by *Acetobacter persici*. The BL-tolerance and the lipid accumulation were dependent on the increment of gut microbiota. Genomic analysis identified mutations in the Hippo signaling pathway linked to midgut elongation, while transcriptome analysis showed downregulation of *Tachykinin* (*Tk*), a key suppressor of intestinal lipogenesis. Genetically induced lipid accumulation through manipulation of *Tk* or related lipogenic genes was sufficient to confer BL-tolerance. Moreover, our findings indicate that parental BL irradiation, along with accumulated mutations from laboratory selection, played a crucial role in midgut elongation and increased bacterial abundance. These findings reveal evolutionary responses to excessive BL exposure that shape host traits to maximize the benefits provided by gut microbiota.

Introduction

Organisms utilize various environmental cues for survival, yet excessive exposure to these cues can act as stressors. Toxicity resulting from environmental stressors impacts the fitness and evolution of organisms.

Blue light (BL) within the 400-500 nm range, abundant in sunlight, is crucial for insect physiology and ecology, influencing processes such as visual perception, circadian rhythms, and photoreactivation (Fig. 1a)[1–4]. However, excessive BL exposure is lethal across various insect species, with toxicity varying by species and developmental stage[5,6]. Our previous studies have demonstrated that exposure to BL at intensities below 40 % of sunlight's BL content for several days can be lethal to various insects[5–7]. Notably, in some species, BL is more lethal than ultraviolet A (315-400 nm) or shorter-wavelength BL near 400 nm[5–7]. In *Drosophila melanogaster* (hereinafter referred to as *Drosophila*), BL around 465 nm is particularly toxic to both pupae and adults, with males being more sensitive than females[5].

The underlying mechanism of BL toxicity likely involves oxidative stress induced by reactive oxygen species (ROS) generated by mitochondria and other cellular components, leading to organ damage[5,8–12]. While the physiological mechanisms of BL toxicity are increasingly understood, the evolutionary responses to this stressor remain poorly characterized.

Laboratory selection has contributed to understanding the evolutionary responses of organisms to environmental stressors[13,14]. *Drosophila* is well-applied for laboratory selection experiments[15]. Importantly, these experiments often reveal evolutionary responses that were not anticipated at the outset. For example, laboratory selection has demonstrated trade-offs such as increased cold stress resistance accompanied by reduced fecundity and has identified shared proteomic evolutionary changes across various stressors[16,17]. Therefore, *Drosophila*-based laboratory selection is a valuable tool for investigating evolutionary responses to environmental stress.

In this study, we established *Drosophila* lines with BL-tolerance through laboratory selection across consecutive generations to characterize the acquired phenotypes. By characterizing the selected line (SL) flies in terms of morphological, physiological, and genetic traits, we

found that the gut-microbiota mediated lipid accumulation is a key adaptive trait for enhanced BL-tolerance.

Result

Drosophila evolved BL-tolerance through laboratory selection

We generated a *Drosophila* line with BL-tolerance using laboratory selection. Specifically, we selected *Drosophila* adults that exhibited low impact following BL irradiation and conducted artificial selective breeding to develop BL-tolerant lines (Fig. 1b). After a 3-day BL irradiation and a 2-day recovery period, we conducted a climbing assay and classified individuals capable of climbing as low impact. BL irradiation was performed at around 470 nm, the wavelength most toxic to *Drosophila* adults, with a photon flux density where approximately 50 % of individuals exhibited low impact (Supplementary Fig. 1a)[5]. The un-selected control line (UCL), maintained without BL irradiation, served as a negative control for comparative analyses with the SL (Fig. 1b). This procedure was replicated in three independent lines for each regime.

Generally, BL irradiation negatively affected *Drosophila* fecundity, strongly inhibiting ovarian development (Fig. 1c). However, in SL flies, improved adaptability was evident after over 20 generations of selection, where fecundity and ovarian development was maintained despite BL irradiation (Fig. 1-f and Supplementary Fig. 1b). On the contrary, fecundity of SL flies increased in response to BL irradiation, whereas UCL flies showed reduced fecundity (Fig. 1f). Additionally, the lifespan of SL flies under continuous BL irradiation was longer than that of UCL flies (Fig. 1h). These results collectively suggest that we have successfully established a new *Drosophila* line (SL) with BL-tolerance.

SL flies exhibited obese phenotype, lipid accumulation, and oxidative stress resistance

Next, we examined the phenotypic characteristics of SL flies exhibiting BL-tolerance. We noticed that the SL flies exhibited an obese phenotype characterized by abdomen bloating

93 (Fig. 2a). This led us to hypothesize that these flies might be undergoing lipid accumulation.
94 SL flies are characterized by increased body weight and a developed fat body with
95 numerous lipid droplets (Fig. 2 b-d). They also showed an elongated midgut, and reduction
96 in wing length (Fig. 2 e and Supplementary Fig. 2 a and b). Unexpectedly, we observed low
97 number of oocytes in the SL flies despite increased fecundity upon BL irradiation (Fig 1g
98 and Supplementary Fig. 2c) and strong inter-individual correlation among oocyte number
99 and body weight in the UCL flies (Supplementary Fig 2 d). These results suggest that,
100 without BL irradiation, energy sources are preferentially allocated to the fat body and
101 midgut rather than to oocyte development. We did not find physical traits associated with
102 light reflection through cellular melanin, despite previous reports suggesting these as
103 adaptive traits to phototoxicity (Supplementary Fig. 3)[18].
104 SL flies were rich in major lipids, including fatty acids (fatty acid methyl esters) and
105 triacylglycerol (TAG), and showed starvation resistance, providing evidence of lipid
106 accumulation (Fig. 2f-h). The lipid droplets and their constituent TAG have been suggested
107 to protect against oxidative damage[19–21]. Consistent with these findings, SL flies displayed
108 higher oxidative stress resistance than UCL flies (Fig. 2i).
109

110 **Increased bacterial abundance in SL flies**

111 It has been reported that host lipid homeostasis is linked to gut microbiota-derived
112 acetate[22,23]. Acetate is converted to acetyl-CoA, which serves as a substrate for de novo
113 lipogenesis[24,25]. Given this insight and considering the elongated midgut in SL flies
114 accumulating lipids, we investigated gut microbiota profiles in SL and UCL flies. In both flies,
115 16S rRNA gene sequencing of whole body DNA revealed that a single species of *Acetobacter*
116 (*Acetobacter persici)*, a common gut bacteria in *Drosophila*, dominated (>99 %) the
117 microbiota (Supplementary Fig. 4a)[26]. Notably, higher bacterial counts were obtained in SL
118 flies compared to UCL flies, and a positive correlation was observed between body weight
119 and bacterial abundance, although the microbiota profile remained unchanged (Fig. 3a and
120 Supplementary Fig. 4b and c). Since all randomly sequenced colonies were identified as *A.*

121 *persici*, the difference in bacterial abundance between SL and UCL flies is likely to reflect the
122 gut colonization level of this bacterium (Supplementary Table 11).
123

124 **Gut microbiota promotes BL-tolerance and lipid accumulation in SL flies**

125 Following BL irradiation, both bacterial abundance and body weight in SL flies drastically
126 decreased (Fig. 3b and c), suggesting that these flies might utilize gut microbiota for BL-
127 tolerance. Consistently, acetic acid bacteria, including *Acetobacter*, which metabolizes
128 acetate, are known to influence fecundity and TAG levels in *Drosophila*[23,27–34]. We tested the
129 hypothesis that gut microbiota plays a role in shaping the phenotype of SL flies using an
130 antibiotic mixture (Abx) (Supplementary Fig. 5a).
131 We investigated the impact of restoring gut microbiota on BL-tolerance in SL flies by infecting
132 Abx-treated flies with gut contents. We examined the effects on body weight, climbing ability,
133 fecundity, and emergence rate. The fecundity and emergence rate of Abx-treated SL flies
134 were inhibited by BL irradiation (Fig. 3d). Infection of Abx-treated SL flies with gut contents
135 from SL flies rescued these phenotypes (Supplementary Fig. 4b-d and Fig. 3d). In contrast,
136 infection with gut contents from UCL flies barely rescued the phenotypes in Abx-treated SL
137 flies (Supplementary Fig. 5a-c and Fig. 3e). Without irradiation, non-treated SL flies showed
138 lower fecundity than UCL flies, whereas Abx-treated SL flies displayed fecundity equivalent
139 to UCL flies (Fig. 3e).
140 Consistently, Abx treatment significantly impacted the body weight of SL flies, with elevated
141 TAG levels observed only in non-treated flies (Fig. 3e and f). Non-treated SL flies maintained
142 higher body weight than non-treated UCL flies despite similar food consumption levels (Fig.
143 3g and Supplementary Table 3). This result highlights the dependence of SL flies' body
144 weight and lipid accumulation on their gut microbiota.
145 Furthermore, the midgut of Abx-treated SL flies was smaller than that of non-treated SL flies
146 but longer than that of UCL flies, with a positive correlation observed between body weight
147 and midgut length (Fig. 3h and Supplementary Fig. 6). Enhanced oxidative stress resistance
148 was observed only in non-treated SL flies (Supplementary Fig. 7a and b). These observations

149 align with previous reports that gut microbiota is linked to gut morphology and oxidative stress
150 resistance[26,35,36]. Overall, these results suggest that the characteristic phenotype in SL flies
151 is shaped by their gut microbiota.
152

153 **Host genome and transcriptomic profiles explain the characteristic**
154 **phenotype of SL flies**

155 To investigate whether SL flies develop their phenotypes through interactions with gut
156 microbiota, we conducted comparative genomic analyses of UCL and SL flies. First, we
157 performed variant discovery using whole genome sequencing to detect common variants
158 selected in SL flies. Homozygous variants shared among the three replicate lines in each
159 regime and absent in Canton-S were identified. SL-specific SNPs and indels were detected
160 in 633 and 1936 genes, respectively. A total of 2224 genes were found to have SL-specific
161 variants, with the majority located outside the coding sequences (CDS) (Fig. 4a). Enrichment
162 analysis using the Kyoto Encyclopedia of Genes and Genomes (KEGG) identified the Hippo
163 signaling pathway as the only significantly enriched pathway (Fig. 4b).
164 The Hippo signaling pathway regulates intestinal elongation[37,38]. The presence of Hippo
165 pathway-regulated genes (*Par-1*, *Misshapen*) among CDS variants[38–40], along with the
166 elongated midgut observed in Abx-treated SL flies, suggests that midgut elongation in SL
167 flies is potentially influenced by these variants (Supplementary Table 12 and Fig. 3h).
168 Variants located outside of the CDS are generally thought to influence gene expression, and
169 gut microbiota may alter host phenotypes through changes in the host transcriptome[41]. We
170 performed transcriptome analysis on the whole body of non-irradiated UCL and SL flies by
171 RNA sequencing and compared gene expression profiles between non-treated and Abx-
172 treated flies. We identified 1242 differentially expressed genes (DEGs), with 1192 (96 %)
173 specific to non-treated SL flies (Fig. 4c and Supplementary Fig. 8 and Supplementary Table
174 13). KEGG analysis of the 1192 DEGs revealed gene enrichment in oxidative
175 phosphorylation, metabolic pathways, Toll and Imd signaling, and the TCA cycle (Fig. 4d).
176 Suppressed mitochondrial metabolism is known to lead to lipid accumulation in various

177 animal species[42,43]. Non-treated SL flies showed broad downregulation of oxidative
178 phosphorylation and the TCA cycle, which are associated with mitochondrial metabolism (Fig.
179 4e). Several genes, whose downregulation is known to induce lipid accumulation, were also
180 specifically downregulated in non-treated SL flies (Fig. 4e)[44–46]. Among those, *Tachykinin*
181 (*Tk)* was also identified in the genome sequencing as variants exhibited specific
182 downregulation in non-treated SL flies (Fig. 4e). In addition, *Tk* expression is known to be
183 modulated in response to acetate produced by gut microbiota, thereby regulating lipid
184 utilization in enterocytes[23,47]. These results suggest that the phenotypes of SL flies are
185 shaped through interactions with their gut microbiota.
186

187 **Lipid accumulation via genetic manipulation confers BL-tolerance**

188 To prove the causal-relationship between the lipid accumulation and BL-tolerance, we
189 examined the BL-tolerance in genetically manipulated flies that are reported to increase the
190 TAG level [41,42]. We employed a range of mutants and GAL4/UAS-mediated manipulations,
191 including knockdown of *Tk*, *Adipokinetic hormone receptor* (*AkhR*), and *Lipid storage dloplet-*
192 *1* (*Lsd1*), which were downregulated in the SL flies (Fig. 4). Interestingly, knocking down
193 these genes resulted in particularly enhanced BL-tolerance, to a comparable level to the SL
194 flies (Fig. 5a). Furthermore, we also observed enhanced BL-tolerance by other genetic
195 manipulations, such as knockdown of *Brummer* (*Bmm*), *Phosphatase and tensin homolog*
196 (*Pten*), and *Stromal interaction molecule* (*Stim*), and overexpression of *Insulin-like receptor*
197 (*InR*), *Lk6 kinase* (*Lk6*), and *Lipid storage droplet-2* (*Lsd2*). Indeed, we found a significant
198 positive relationship between fecundity and TAG levels was observed (Fig. 5b), strongly
199 suggesting that lipid accumulation in general is a trait that confers BL-tolerance.
200

201 **Parental BL irradiation affects progeny's gut microbiota-associated traits**

202 Finally, we investigated why only the gut microbiota from SL flies could rescue BL-tolerance
203 in infection experiments, despite the dominance of the same gut bacterial species across
204 regimes (Supplementary Fig. 4a and Fig. 3e). We hypothesized that parental BL irradiation

205 might impact gut microbiota-associated traits (e.g., increased bacterial abundance) in the
206 progeny.
207 To test this hypothesis, we examined the phenotypes (body weight, BL-tolerance) in Abx-
208 treated SL flies that had regained gut microbiota through inoculation with gut contents from
209 flies with different parental experiences. Abx-treated SL flies inoculated with gut contents
210 from SL flies whose parents had experienced BL irradiation showed the greatest increase in
211 body weight (Supplementary Fig. 9a). However, flies inoculated with different *A. persici*
212 cocktails, each standardized in concentration, exhibited similar body weight increases
213 (Supplementary Fig. 9b). This suggests that quantitative rather than qualitative changes in
214 gut microbiota due to parental BL irradiation are responsible for the increases in host body
215 weights.
216 Furthermore, gut contents from UCL flies whose parents had experienced BL irradiation also
217 rescued the phenotypes of Abx-treated SL flies, restoring fecundity to the level conferred by
218 gut contents from SL flies (Fig. 6a). These results indicate that parental BL irradiation affects
219 the progeny's gut microbiota-associated traits. Consistently, parental BL irradiation increased
220 the progeny's body weight, bacterial abundance, and midgut length in both UCL and SL flies
221 (Supplementary Fig. 10 and Fig. 6b, c). Notably, even without parental BL irradiation, the
222 midgut of SL flies was longer than that of non-irradiated UCL flies, suggesting that this
223 inherited trait has been conserved during the laboratory selection of SL flies (Fig. 6c). Given
224 that parental BL irradiation leads to an increase in bacterial abundance in progeny, the
225 different outcomes observed in gut content inoculation experiments likely reflect variations in
226 bacterial loads.
227

228 ## Discussion

229 In this study, we established a BL-tolerant *Drosophila* line through laboratory selection,
230 demonstrating that excessive BL irradiation over generations drives the evolution of adaptive
231 traits, particularly gut microbiota-mediated lipid accumulation. This supports the increasingly
232 recognized role of microbiota in host adaptation to environmental stress, where specific

233 bacterial populations expand under laboratory-driven selection pressures, contributing to
234 adaptive host phenotypes[32,48–51]. Our findings further reveal that the elongation of the host
235 gut in response to BL toxicity facilitates an increase in beneficial bacteria, ultimately
236 enhancing host fitness under excessive BL exposure.
237 SL flies exhibited increased lipid accumulation (Fig. 2), and genetic manipulation to increase
238 lipid conferred BL-tolerance (Fig. 5). Acquisition of BL-tolerance through lipid accumulation
239 can be explained by its role in protecting against ROS, which is produced upon BL
240 irradiation[10,11]. Intracellular lipid droplets play a critical role in shielding cells from the oxidative
241 stress, as reduced TAG levels are associated with increased sensitivity to such stress[19–21,52].
242 The accumulation of lipid droplets in response to intracellular ROS has been observed in
243 many species[21,52]. Additionally, lipid droplets are closely linked to fecundity, as higher TAG
244 levels are associated with improved fecundity, whereas reduced TAG levels can lead to
245 oocyte degeneration[53,54]. Thus, lipid accumulation not only helps defend against BL toxicity
246 but also supports the maintenance of fecundity. Furthermore, the transcriptome of SL flies
247 revealed a broad downregulation of mitochondrial metabolism (Fig. 4e). Mitochondria, while
248 crucial for energy production, also contribute to ROS generation[55]. Therefore, the inhibition
249 of mitochondrial metabolism and lipid utilization could be an adaptive strategy to accumulate
250 lipids while minimizing oxidative stress.
251 We identified *Acetobacter persici* as the predominant bacterial species, and showed the
252 critical role of their increased abundance in the acquisition of BL-tolerance. *Acetobacter*
253 species are well-known symbionts of *Drosophila* and other insects[56], recognized for their
254 acetate production. Acetyl-CoA, derived from acetate, is essential for lipid utilization[25,57] and
255 also plays a crucial role in the acetylation of both histone and non-histone proteins, facilitating
256 adaptive responses through tissue plasticity[23,58,59]. The elevated TAG levels observed in SL
257 flies may be explained by the increased acetyl-CoA pool resulting from gut microbiota-
258 derived acetate. Additionally, gut microbiota might act as a barrier against physiological
259 stress induced by BL toxicity. The significant reduction in gut microbiota following BL
260 irradiation in SL flies (Fig. 3b) suggests the evolution of mechanisms that utilize bacteria as

261 a buffer against BL toxicity or as a direct nutritional resource. This finding aligns with previous
262 research showing that *Acetobacter* enhances the fecundity and stress tolerance of the host
263 fly[26,32–34].
264 The increase in bacterial abundance appears to be associated with midgut elongation and
265 genetic changes, particularly those in the Hippo signaling pathway (Fig. 3h and Fig. 4b). We
266 also found that the parental irradiation to BL, in addition to the accumulated mutations, is
267 critical for the midgut elongation and bacterial abundance (Fig. 6b and c). In *Drosophila*, the
268 midgut undergoes plastic elongation or shortening in response to environmental
269 conditions[60,61]. This physical expansion of the gut, which increases spatial capacity, offers
270 several advantages, including more efficient nutrient absorption, increased bacterial
271 abundance, and maintenance of gut homeostasis[53,62–66]. However, midgut elongation alone,
272 even after one generation of parental exposure to BL toxicity, is insufficient for BL-tolerance
273 (Fig. 1d and Fig. 6c). Full BL-tolerance requires both midgut enlargement and specific genetic
274 changes. Among these genetic factors, the neuropeptide *Tk* and its receptor *TkR99D* are
275 particularly important (Fig. 5 and Supplementary Table 12), as they may regulate lipid
276 utilization in response to acetate produced by the gut microbiota[23,46].
277
278 Parental exposure to environmental stressors, such as starvation, has been reported to
279 induce epigenetic inheritance, altering the information passed to progeny[67]. Similarly,
280 parental BL exposure may have led to epigenetic modifications that influence gut microbiota-
281 associated traits in the progeny. This proposed mechanism is consistent with evidence that
282 parental BL irradiation affects the progeny's transcriptome[68].
283
284 To conclude, our findings highlight that lipid accumulation mediated by gut microbiota is a
285 critical adaptive trait for BL-tolerance. The elongation of the midgut, associated with
286 increased bacterial abundance, emerges as a key factor in this adaptation, may drive by
287 genetic and epigenetic changes from selective pressures and parental experience of BL
288 toxicity. These evolutionary responses to excessive BL exposure demonstrate how host traits

evolve to maximize the benefits provided by gut microbiota.

Methods

Fly cultures and diet

Flies were maintained at 23-26 °C on a 16:8 hour light-dark cycle using cold cathode fluorescent lamps as the light source. Detailed lighting conditions are provided in the Supplementary Table 14.

The fly diet consisted of 5 g glucose (Fujifilm Wako Pure Chemicals Co., Osaka, Japan), 6 g dry brewer's yeast (Asahi group holdings Ltd., Tokyo, Japan), 1 g agar (Fujifilm Wako Pure Chemicals Co.), 0.4 mL propionic acid (Fujifilm Wako Pure Chemicals Co.), 0.4 mL 70 % ethanol (Fujifilm Wako Pure Chemicals Co.), 0.01 g butyl p-hydroxybenzoate (Fujifilm Wako Pure Chemicals Co.), and 100 mL distilled water.

Blue light (BL) irradiation

We previously reported that blue light at around 465 nm exhibits high toxicity to adult *Drosophila*, with males being more sensitive than females[5]. Unless otherwise specified, flies were exposed to 462 nm BL for 3 days. Virgin flies aged 1-5 days were collected for experiments. BL irradiation conditions varied across experiments:

Fig. 1c-g, 3d, 6a-c: Photon flux density 10.3×10^{18} photons·m^{-2}·s^{-1} (approximately 175 μmol·m^{-2}·s^{-1}, 20,000 Lux) for females.

Fig. 5: 465 nm BL, photon flux density 9.5×10^{18} photons·m^{-2}·s^{-1} (approximately 19,500 Lux) for females.

Fig. 1c-g, Fig.6b and c: Photon flux density 6.5×10^{18} photons·m^{-2}·s^{-1} (approximately 122 μmol·m^{-2}·s^{-1}, 13,500 Lux) for males.

Fig. 1h: Photon flux density 8×10^{18} photons·m^{-2}·s^{-1} for males and 10×10^{18} photons·m^{-2}·s^{-1} for females.

For details in Supplementary Table 15.

Irradiation was performed in a multi-room incubator (LH-30CCFL-8CT; Nippon Medical & Chemical Instruments Co., Ltd, Osaka, Japan) at 24-26 °C, with LED panels (IS-mini®, ISL-150 × 150 Series; CCS Inc., Kyoto, Japan) installed on the ceiling. Photon flux density was

measured using a high-resolution spectrometer HSU-100S (Asahi Spectra Co., Ltd., Tokyo, Japan) with ND 0050 filter (Asahi Spectra Co., Ltd), lux meter LX-90 (AMTAST USA Inc., Florida, USA) and spectroradiometer MS-730 (EKO Instruments Co., Ltd., Tokyo, Japan).

Laboratory selection for BL-tolerance

Artificial selection

We used the Canton-S strain of *Drosophila*, a common wild-type strain, as the ancestral population for laboratory selection. Two regimes were established: a selected line (SL) subjected to BL toxicity every generation, and an un-selected control line (UCL). Each regime included three replicate lines. The UCL, used as a negative control group, was kept in darkness for 3 days. For each regime, 60-100 virgin flies aged 1-5 days were placed in two 60 mm × 90 mm glass Petri dishes for BL irradiation. Because blue light at around 470 nm highly toxicity to adult, SL and UCL flies (positive control group) were exposed to 462 nm BL for 3 days[5].

Climbing assay

Following irradiation, flies were placed in a breeding environment (for details, see “Fly cultures and diet” in Methods) for a 2-day recovery period. For the data shown in Supplementary Fig. 1a, the impact of BL toxicity was assessed based on a 4-minute climbing assay and categorized into five states:

“Low impact” (capable of climbing):

1. Intact; Climbing >2 cm (as defined from the 17th generation onwards)
2. Semi-intact; Capable of climbing, but less efficiently

“High impact” (unable to climb):

3. Phase1; Alive but unable to climb
4. Phase2; Non-ambulatory
5. Phase3; Dead

Artificial selective breeding and evaluation of fecundity

Following the climbing assay, SL individuals classified as "Low impact" were allowed 5 days

347 for mating and egg-laying. Each 3 mL diet medium vial contained 9-13 pairs, with a total of
348 4-8 vials (for details, see Supplementary Table 16). After 5 days, the diet medium
349 containing eggs and larvae was transferred to a larger plastic box (40 mL diet medium, 72
350 × 72 × 100 mm; Insect Breeding Square Dish, SPL Life Sciences, Gyeonggi-do, Korea) to
351 ensure sufficient food supply. One box was used for every 4-5 vials. UCL parents were
352 randomly chosen from the negative control group (for details, see "Laboratory selection for
353 BL-tolerance -Artificial selection-" in Methods) and reared under the same conditions as the
354 SL flies. The total number of pupae was counted and divided by the number of parents to
355 determine the fecundity per female for each generation.
356

357 **Survival assays**

358 Survival assays were conducted for three different stress conditions: continuous blue light
359 irradiation, starvation, and oxidative stress. For all assays, virgin female flies aged 5-10
360 days were used. The number of surviving individuals was manually counted every 2 hours
361 for all assays.
362 For the continuous BL irradiation assay in Fig.1h, flies were exposed to 462 nm blue light.
363 Fifty or forty-two flies were placed in each glass petri dish containing standard diet medium.
364 For the starvation and oxidative stress assays, ten flies were placed in each vial. For the
365 starvation assay in Fig.2h, flies were placed in vials containing a medium composed of 1%
366 (w/v) agar (Fujifilm Wako Pure Chemicals Co.) in distilled water.
367 For the oxidative stress assay, flies were placed in vials containing a medium prepared with
368 either 10 mM Paraquat dichloride standard (Fujifilm Wako Pure Chemicals Co.) (Fig. 2i) or
369 10 mM 1,1'-Dimethyl-4,4'-bipyridinium Dichloride (Tokyo Chemical Industry Co., Ltd.,
370 Tokyo, Japan) (Supplementary Fig. 7a and b), 5% (w/v) glucose (Fujifilm Wako Pure
371 Chemicals Co.), and 1% (w/v) agar (Fujifilm Wako Pure Chemicals Co.) in distilled water.
372

373 **Measurement of fecundity**

374 To measure fecundity (Fig. 1g, Fig. 3d, Fig.5 and Fig. 6a), after 3 days of dark conditions
375 (non-irradiation) or BL irradiation followed by a 3-day recovery period, 5 surviving females
376 were randomly chosen and mated with 5 non-irradiated virgin males (aged 1-10 days) in
377 individual pairs within 5 mL diet medium vials for 4 days of egg-laying. The total number of
378 pupae and emerged adults were counted to evaluate fecundity and emergence rate (Fig.
379 1g measured only the total number of pupae).
380 Fig. 1g utilized non-irradiated males corresponding to the UCL or SL regime, Fig. 5 used
381 non-irradiated Canton-S males, and Fig. 3d and Fig. 6a employed non-irradiated males
382 treated with an antibiotic mixture corresponding to the UCL or SL regime.
383

384 **Measurement of body weight and organ size**

385 Virgin flies aged 4-12 days were collected and anesthetized by chilling on ice for all
386 measurements. Body weight was measured using an AUW220D balance (Shimadzu,
387 Kyoto, Japan) for experiments in Fig. 2b, 3c, 3e, Supplementary Fig. 2a, Supplementary
388 Fig. 5b, Supplementary Fig. 2a, Supplementary Fig. 6, Supplementary Fig. 9a,
389 Supplementary Fig. 9b and Supplementary Fig. 10.
390 For experiments in Fig. 1c, Fig. 1e, Supplementary Fig. 2b and Supplementary Fig. 2c,
391 wings or ovaries were dissected and photographed using a SteREO Discovery.V12
392 stereomicroscope and an Axiocam 305 color camera (Carl Zeiss, Oberkochen, Germany).
393 Wing length was measured as the distance between the alula opening and the distal edge
394 of the 3rd longitudinal vein, using Fiji ImageJ2 (version 2.3/1.54f), following the previous
395 method[69]. The number of stage 14 oocytes was counted under the microscope. In Fig. 2e,
396 Fig. 3h and Fig. 6c, midgut lengths of the R1-R5 regions were manually measured from the
397 midgut images using Fiji ImageJ2[66].
398

399 **Lipid droplet staining and imaging**

400 We performed dissection and fluorescence microscopy to visualize lipid droplets in the fat
401 body of the abdominal epithelium from virgin female flies aged 6-12 days. After removing

402 other tissues from the abdomen, we fixed the abdominal epithelium in PBS containing 4 %
403 paraformaldehyde (Fujifilm Wako Pure Chemicals Co.) for 20 minutes. After fixation, we
404 washed the samples twice with PBS (Gibco, Carlsbad, USA) for 15 minutes each. The fixed
405 abdominal epithelium was stained with Nile Red (Fujifilm Wako Pure Chemicals Co.) at a
406 concentration of 10 μg/mL overnight according to previous study[70]. Following this, we
407 washed the samples twice with PBS for 10 minutes each and then stained them with
408 NucBlue (Thermo Fisher Scientific, Waltham, MA, USA) for 3 minutes, followed by a 5-
409 minute wash with PBS. All staining procedures were conducted in a light-shielded
410 environment at room temperature. Imaging was performed using an ECLIPSE Ti2
411 microscope and a DS-Ri2 camera (Nikon, Tokyo, Japan). The images were analyzed using
412 the Python package OpenCV (Python version 3.8.3 version 4.5.3.56) to obtain the mean
413 fluorescent intensity of Nile Red.
414

415 **Lipid extraction and derivatization of fatty acids**

416 We homogenized 2 virgin female flies aged 6-12 days in 100 μL of PBS (Gibco). Lipids
417 were extracted using the Bligh and Dyer method[71,72]. To the homogenate, we added 600 μL
418 of methanol (Fujifilm Wako Pure Chemicals Co.) and chloroform (Fujifilm Wako Pure
419 Chemicals Co.) in a 2:1 (v/v) ratio, vortexed for 1 minute, and then shook at 1,000 rpm at
420 4°C for 2 hours. Next, we added 200 μL of chloroform and 250 μL of distilled water to the
421 mixture, vortexed for 1 minute, and centrifuged at 9,000 rpm for 2 minutes to separate the
422 phases. The organic lower phase was collected. We then added an additional 400 μL of
423 chloroform to the remaining mixture, vortexed for 1 minute, and centrifuged at 9,000 rpm for
424 2 minutes to achieve phase separation. The two organic extracts were pooled, the
425 container was sealed, and the extracts were dried under vacuum. The dried lipids were
426 derivatized using the Fatty Acid Methylation Kit (Nacalai Tesque, Inc., Tokyo, Japan) and
427 the Fatty Acid Methyl Ester Purification Kit (Nacalai Tesque, Inc.) according to the kit
428 protocols. Fatty acid methyl esters (FAMEs) were collected.
429

430 **Gas chromatography-tandem mass spectrometry (GC-MS/MS) analysis**

431 The FAMEs were analyzed using a GCMS-QP2010 Ultra (Shimadzu) equipped with a DB-5
432 ms column (30 m × 0.25 mm ID, 0.25 μm film thickness) (J&W Scientific, Folsom, USA).
433 The carrier gas used was helium at a pressure of 100 kPa. The analysis conditions were as
434 follows:
435 The column oven was set to an initial temperature of 40°C and held for 5 minutes. The
436 temperature was increased at a rate of 10°C/min to 280°C and maintained at 280°C for 10
437 minutes. The injection port temperature was set to 220°C, and the analysis was performed
438 in split mode.
439 Fatty acids were identified using a similarity search against the standard substance
440 Supelco F.A.M.E. Mix C4-C24 (Supelco, Bellafonte, PA, USA) and relevant references[73,74].
441 The total ion chromatogram area for each compound was measured.
442 Based on the obtained data, we compared the total amount of FAMEs. The log-transformed
443 average values of each compound in each replicate line were visualized using a cluster
444 map. Clusters were classified by hierarchical clustering using the Ward method, based on
445 Euclidean distances of compound amounts[75].
446

447 **Measurement of triacylglycerol (TAG)**

448 Relative TAG levels were measured by homogenizing 10 virgin female flies (aged 6-12
449 days) in 1000 μL of PBS (Fujifilm Wako Pure Chemicals Co.) containing 0.1% Triton X-100
450 (Nacalai Tesque Inc.). The homogenate was heated at 70°C for 10 minutes and then
451 centrifuged at 20,000 × g for 15 minutes at 4°C. A 10 μL aliquot of the supernatant was
452 used for TAG measurement using the LabAssay Triglyceride kit (Fujifilm Wako Pure
453 Chemicals Co.). For protein normalization, protein concentration was measured using the
454 Bradford method with the Protein Assay CBB Clean Up Kit and Protein Assay CBB Solution
455 (both from Nacalai Tesque Inc.), with the standard calibration curve prepared using
456 Albumin, Bovine Serum, Solution (Nacalai Tesque Inc.). Absorbance was measured using
457 the BioTek Synergy H1 Multimode Reader (Agilent Technologies Inc., Santa Clara, USA).

458 Relative TAG levels were normalized to protein content, adjusted based on the average
459 values from UCL (Fig. 2g and Fig. 5) or non-treated UCL (Fig. 3f), and the Log_2 fold change
460 was computed accordingly.
461

462 **Measurement of reflectance and transmittance**

463 Virgin female flies aged 6-12 days were collected and anesthetized on ice. The abdominal
464 reflectance and transmittance were measured by capturing hyperspectral images using a
465 BX51WI microscope (Olympus, Tokyo, Japan) fitted with an SC-108 hyperspectral imaging
466 system (EBA Japan Co., Ltd., Tokyo, Japan).
467

468 **DNA extraction**

469 DNA was extracted from virgin female flies aged 5-8 days using the DNeasy Blood &
470 Tissue Kit (Qiagen, Hilden, Germany). For both Fig. 4a and Supplementary Fig. 3a, the
471 same sample of 30 flies was used, with 10 flies specifically used for Supplementary Fig. 3c.
472 The surface of the flies was first washed in a 1.5 mL tube with 99 % ethanol (Fujifilm Wako
473 Pure Chemicals Co.) for 30 seconds. Then, 180 μL of PBS (Fujifilm Wako Pure Chemicals
474 Co.) and beads were added, and the flies were homogenized at 3500 rpm for 30 seconds
475 using the Micro Smash MS100R (Tomy Seiko Co., Ltd., Tokyo, Japan) while keeping the
476 mixture cold. Following homogenize, DNA extraction was performed according to kit
477 protocols.
478

479 **16S/ITS rRNA amplicon sequencing (V3-V4 hypervariable region)**

480 Quality checks were performed using the BioAnalyzer, followed by library preparation with
481 the NEBNext® Ultra™ II DNA Library Prep Kit (Illumina, San Diego, CA, USA). Sequencing
482 was conducted on an Illumina NovaSeq 6000 with the following parameters: paired-end
483 reads of 250 bp × 2 (PE250) and an output of 50,000 reads per sample. In silico analyses
484 were performed on a Mac OS (Catalina version 10.15) terminal using Jupyter Notebook
485 (Python version 3.9 version 6.4.11). Quality assessment was conducted with FastQC

486 (version 0.11.8). Data analysis was carried out using QIIME 2 (version 2023.7) with the
487 Silva 138 99% OTUs full-length database (MD5: b8609f23e9b17bd4a1321a8971303310).
488 The QIIME dada2 denoise-paired parameters were set as follows: --p-n-threads 0, --p-trim-
489 left-f 30, --p-trim-left-r 30, --p-trunc-len-f 250, and --p-trunc-len-r 250. Operational
490 Taxonomic Unit sequences were classified to determine the gut microbiota composition.
491

492 **Bacterial abundance and identification**

493 Body weight (4 virgin adult females) measurements were conducted following either non-
494 irradiation or BL irradiation. In Fig. 3b, after 3 days of BL irradiation followed by a 3-day
495 recovery period, 4 surviving females were randomly chosen and virgin female flies, aged 5-
496 8 days, were surface-sterilized by immersion in 70 % ethanol for 1 minute, followed by
497 three washes with PBS (Fujifilm Wako Pure Chemicals Co.). The flies were homogenized
498 in 500 μL of PBS in a 2 mL tube to produce a stock solution, which was then diluted 1:10
499 with PBS. A 10 μL aliquot of the diluted solution was plated onto MRS agar plates
500 (comprising 5.5 g MRS broth (Becton, Dickinson and Company, Franklin Lakes, NJ, USA),
501 1 g agar (Fujifilm Wako Pure Chemicals Co.), and 100 mL distilled water). Colony-forming
502 units (CFU) were counted after 72 hours of incubation at 30-31 °C. In Fig.3 a, fold change
503 values are calculated based on the mean of the corresponding UCL replicate line. In Fig.3
504 b, $\log_2$ fold change values are calculated based on the mean of the corresponding non-
505 treated UCL replicate line. In Fig. 6a, fold change values are calculated based on the mean
506 of the corresponding UCL non-experience.
507 Following CFU measurement, single colonies were isolated for identification. The 16S
508 rRNA genes of isolated bacterial strains were amplified by PCR using universal bacterial
509 primers 27F and 1492R. Sequencing was performed on an ABI3500 Sanger sequencing
510 platform (Thermo Fisher Scientific) using the BigDye™ Terminator v1.1 Cycle Sequencing
511 Kit (Thermo Fisher Scientific)[76,77].
512

513 **Antibiotic mixture treatment**

514 The antibiotic mixture (Abx) was prepared according to established protocols[78]. Flies were
515 reared on a diet containing Abx from the embryo stage to adult. The diet was supplemented
516 with 100 μg/mL streptomycin sulfate (Fujifilm Wako Pure Chemicals Co.), 50 μg/mL
517 tetracycline hydrochloride (Fujifilm Wako Pure Chemicals Co.), and 200 μg/mL rifampicin
518 (Fujifilm Wako Pure Chemicals Co.).
519

520 **Capillary feeding (CAFE) assay**

521 The CAFE assay was conducted using a method adapted from previous research[79]. The
522 feeding solution comprised 5 % sucrose, 2 % yeast extract, 0.25 % nipagin (dissolved in
523 ethanol), 0.005 % red dye, and water. To prevent egg-laying within the capillaries, 4 virgin
524 male flies aged 5-8 days were employed in the experiment. Consumption was measured by
525 allowing the flies to feed for 24 hours.
526

527 **Infection with gut contents or *Acetobacter persici* cocktails**

528 In Fig. 3d, Supplementary Fig. 4b-d, Fig. 6c, and Supplementary Fig. 9a, 30 virgin female
529 flies aged 5-8 days were surface-sterilized by immersion in 70 % ethanol for 1 minute,
530 followed by three washes with PBS (Fujifilm Wako Pure Chemicals Co.). The flies were
531 homogenized in 500 μL of PBS in a 2 mL tube to create a stock solution, which was then
532 diluted 1:10 with PBS.
533 To infect the gut microbiota, 20 μL of the diluted solution was added to the diet, and virgin
534 females aged 1-4 days were maintained on this diet for 4 days. PBS was used as a control.
535 Body weight was measured before and after infection. After 3 days of non-irradiation or BL
536 irradiation followed by a 3-day recovery period, climbing ability and fecundity were
537 evaluated.
538 In Supplementary Fig. 9b, *Acetobacter persici* was cultured and isolated on MRS plates for
539 48 hours. These isolates, along with the standard strain of *A. persici* (JCM 25330), were
540 cultured in 200 μL of MRS broth (5.5 g MRS broth (Becton, Dickinson and Company) and
541 100 mL distilled water) in 96-well plates for 72 hours. The bacterial culture pellet, grown for

542 48 hours in a 96-well plate containing 200 μL of MRS broth per well, was diluted 1:30 with
543 PBS and inoculated into 20 μL of diet. Autoclaved MRS was also diluted 1:30 with PBS,
544 and 20 μL of this mixture was used as the control.
545

546 **Whole-genome resequencing, variant identification, and enrichment**
547 **analysis**

548 Quality checks were performed using a BioAnalyzer, followed by library preparation with
549 the NEBNext® Ultra DNA Library Prep Kit (Illumina). Sequencing was conducted on an
550 Illumina NovaSeq 6000 with the following parameters: paired-end reads of 150 bp (PE150),
551 a data output of 10 G bases per sample, and approximately 66.7 million reads per sample.
552 In silico analyses were performed using macOS (Catalina version 10.15.7) terminal and
553 Jupyter Notebook (Python version 3.9 version 6.4.11). The quality of the fastq files was
554 assessed using seqkit stat (version 0.16.1). Quality assessment was further performed with
555 fastqc (version 0.11.8). Reads were trimmed using trimmomatic (version 0.39) with the
556 following parameters: LEADING:20, TRAILING:20, SLIDINGWINDOW:4:15, and
557 MINLEN:20, based on Illumina adapter sequences (CTGTCTCTTATACACATCT). Trimmed
558 data was re-evaluated with seqkit stat and fastqc to confirm the quality of the trimmed
559 reads.
560 Mapping was performed using the reference genome BDGP6.46, INSDC Assembly
561 GCA_000001215.4 (details provided in the Supplementary Table 12). Indexing and
562 mapping were conducted using bwa (version 0.7.17), followed by conversion from SAM to
563 BAM format using samtools (version 1.10). PCR duplicates were marked with GATK
564 (version 4.2.6.1), and alignment statistics were calculated from the BAM file. Paired-end
565 reads were merged using samtools, and the merged BAM file was sorted.
566 Variant calling was executed with sambamba mpileup and varScan pileup2snp, using the
567 parameters: SNP; --min-coverage 10 --min-var-freq 0.90 --p-value 0.05 (filter; default),
568 Indel; --min-coverage 10 --min-var-freq 0.90 --p-value 0.10 (filter; --min-reads2 4 --min-var-
569 freq 0.15 --p-value 0.05). Homozygous variants were identified by extracting rows with

570 matching Cons and VarAllele values. Common positions across replicates (lines 1, 2, and
571 3) within each regime were defined to identify regime-specific shared variants. Shared and
572 unique variants among UCL, SL, and Canton-S (SRX8038113)[80] were analyzed.
573 Variants were annotated using SnpEff (version 5.0) and visualized using IGV (version
574 2.8.12). Enrichment analysis was conducted with ShinyGO 0.80 and Kyoto Encyclopedia of
575 Genes and Genomes (KEGG), based on the unique variants identified (details in the
576 Supplementary Table 12). Variants classified as having a low impact by SnpEff were
577 excluded from the analysis list (full list available in the Supplementary Table 18).
578

579 **RNA extraction**

580 Ten virgin female flies aged 5-8 days were immediately frozen in liquid nitrogen. The frozen
581 flies were then homogenized in Trizol (Molecular Research Center, Inc, OH, USA).
582 Following homogenization, chloroform (Fujifilm Wako Pure Chemicals Co.) was added to
583 the mixture, which was vortexed twice. The sample was then centrifuged at 20,000 × g for
584 10 minutes at 4°C. The upper aqueous phase was transferred to a new tube, and 200 μL of
585 isopropyl alcohol was added. After vortexing, the mixture was incubated at room
586 temperature for 10 minutes. The sample was centrifuged again at 20,000 × g for 10
587 minutes at 4°C, and the supernatant was discarded. To wash the RNA pellet, 400 μL of
588 75% ethanol (prepared with DEPC-treated water) was added, followed by vortexing. The
589 sample was then centrifuged at 20,000 × g for 5 minutes at 4°C. The supernatant was
590 discarded, and the pellet was centrifuged once more for 1 minute. After allowing the pellet
591 to air-dry, it was resuspended in DEPC-treated water.
592

593 **RNA-sequence and enrichment analysis**

594 Quality assessment was initially performed using a BioAnalyzer. Library preparation was
595 conducted with the NEBNext Ultra II Directional RNA Library Prep Kit (Illumina) and the
596 NEBNext Poly(A) mRNA Magnetic Isolation Module (New England Biolabs, Ipswich, MA,
597 USA). Sequencing was executed on an Illumina NovaSeq 6000, with a read length of

PE150 (150 bp × 2 paired-end), generating a data output of 6 G bases per sample and approximately 40 million reads per sample.

In silico analyses and read trimming followed the protocols described in the " Whole-genome resequencing, variant identification, and enrichment analysis" section. Poly(A) tail removal was performed using cutadapt, and mapping was conducted with hisat2 (version 2.2.1) using the BDGP6.46 reference genome (INSDC Assembly GCA_000001215.4) (for details, see Supplementary Table 19). Gene-wise read counting was accomplished using HTSeq (version 2.0.4) with the dmel-all-r6.54.gtf annotation file. Read count normalization was executed with edgeR (version 3.40.2) using the trimmed mean of M values method. Subsequent principal component analysis and differential expression analysis were carried out with edgeR and scikit-learn (version 1.0.2). Differentially expressed genes (DEGs) were identified by comparing non-treated SL with non-treated UCL, Abx-treated SL, or Abx-treated UCL groups, applying a false discovery rate (FDR)-adjusted p-value threshold of < 0.05. Python libraries such as pandas (version 2.0.3), numpy (version 1.25.2), scipy (version 1.11.2), and stats were used to filter DEGs with p-values below 0.05. For the DEGs, $\log_2$ fold change values and Z-scores normalized within the range of -2 to 2 were calculated. These Z-scores were then used to create a cluster map using the Ward method, classifying genes and treatments based on their similarity patterns.

Enrichment analysis was performed using ShinyGO 0.80. Gene lists related to specific biological functions were curated from KEGG (TCA cycle, oxidative phosphorylation, Toll and Imd signaling pathways) and FlyBase (lipid metabolic processes).

In Fig. 4e, heatmaps illustrating functional profiles were generated using $\log_2$ fold change values. These values were compared for each gene and each group, normalized against the mean value of the non-treated UCL group.

Genetics and evaluate of TAG levels and BL tolerance

We collected genetically engineered flies with known elevated TAG levels and reared them at 23-25°C under a 12-hour light/dark cycle. Using the GAL4/UAS system and null mutants,

we generated flies with RNAi knockdown or overexpression of target genes. The following strains from the Bloomington Stock Center were utilized (see Supplementary Table 5):

Null mutants: *w;Akh* (BL84448), w;*Bmm* (BL15828), *yw,Pdgy* (BL19990), *yw;Chico* (BL14337), *w;InR* (BL8267), *w;Ilp 2 3 5* (BL30889), *w;Lk6* (BL87087)

GAL4 drivers: *yw;Lsp2* (BL6357), *w;ppl* (BL58768), *w;Tk* (BL51973)

UAS strains: *yv;UAS-AkhR*^{RNAi} (BL51710), *yv;UAS-Pect*^{RNAi} (BL63710), *yv;UAS-Pten*^{RNAi} (BL33643), *yv;UAS-Bmm*^{RNAi} (25926), *y sc v sev;UAS-Stim*^{RNAi} (BL52911), *y sc v sev;UAS-Lsd-1*^{RNAi} (BL65020), *yv;UAS-Tk*^{RNAi} (BL25800), *yw;UAS-Gbb* (BL63059), *yw;UAS-InR* (BL8263), *w;UAS-Lsd-2* (BL98116), *w;UAS-Lk6* (BL8709), *w,UAS-Rpr1* (BL5823)

We used F1 progenies for the experiments, obtained by crossing GAL4 driver males with UAS effector females. As controls, we used wild-type Canton-S and w1118 genetically washed with the Canton-S flies, F1 progenies from crosses of w1118 with UAS effectors, and F1 progenies from crosses of GAL4 drivers with *y sc v;eGFP*^{RNAi} (BL41555) and *y sc v;eGFP*^{RNAi} (BL41556) UAS effectors.

Virgin female flies aged 1-5 days were irradiated with either DD or BL for 3 days. Three days after the recovery period, survival rates were assessed, and 5 female flies were randomly chosen to mate with 5 Canton-S males for 4 days (for details, see “Measurement of fecundity” in methods). TAG storage was measured in virgin female flies aged 7-12 days. Relative TAG levels are presented as $\log_2$ fold changes relative to the mean values across all treatments. Fecundity is calculated as $\log_2$ fold changes relative to the non-irradiation condition for each treatment. Data are from SL and UCL (Replicate line 1, Generation 57).

Parental experience of BL irradiation (BL irradiation on the parents)

After 3 days of BL irradiation followed by a 3-day recovery period, flies (male and female) were randomly chosen as parents. These flies were then allowed to mate and lay eggs for 4 days.

Statistical analysis

Bayesian state space model and estimation

In Fig. 1d, intergenerational fecundity data were analyzed using a Bayesian state space model implemented with pystan (Python 3.9, version 2.17.0.0). The Stan model included the following components:

Data block: Defined the number of generations (length of the time series data), a vector of explanatory variables, and three outcome variables corresponding to each replicate line, each following a normal distribution.

Parameters block: Estimated a vector of levels with drift components (mu), vectors of random effects (r1, r2, r3), coefficients of the explanatory variables (b1, b2, b3), the standard deviation representing the magnitude of the drift component (s_z), and the standard deviations of the random effects (s_r1, s_r2, s_r3).

Transformed parameters block: Calculated the expected values for each outcome variable (lambda1, lambda2, lambda3) as the sum of the level with drift component (mu), the product of the explanatory variables' coefficients (b) and values (ex), and the random effects (r).

Model block: Assumed that the random effects followed a normal distribution with a mean of 0 and a given standard deviation. The state equation, mu[i] ~ normal(2 * mu[i-1] - mu[i-2], s_z), expressed changes in the level with drift components using a second-order local linear regression. The observation equations, y1[i] ~ normal(lambda1[i], sigma1), y2[i] ~ normal(lambda2[i], sigma2), and y3[i] ~ normal(lambda3[i], sigma3), defined the observed values as following a normal distribution.

Generated quantities block: Sampled the predicted values for each outcome variable using the normal distribution rather than the Poisson log-link function.

Random numbers were generated according to the posterior distribution using the Markov Chain Monte Carlo (MCMC) method with parameters set to iter=10000, chains=4, and control={'adapt_delta': 0.8, 'max_treedepth': 20}. Convergence was confirmed by ensuring that the *R*hat of the predicted values was <1.10 and by examining the trace plots (for details, see Supplementary Table 20).

Bayesian hierarchical model (HBM)

Unless otherwise specified, hierarchical uncertainty estimation, accounting for random effects, was performed using Hierarchical Bayesian Model (HBM). The model specification and execution utilized the following tools and versions:

Software: R (version 4.0.1), rstan (version 2.32.2, Stan version 2.26.1), brms (version 2.20.4), and bayesplot (version 1.10.0).

Bayesian model comparison: Conducted using Bayes Factor_{10} with the loo function, computing exp(0.5 * (elpd1 - elpd2)), where elpd1 denotes the model's expected log pointwise predictive density (elpd_loo) and elpd2 denotes that of the null model.

MCMC sampling: Parameters were set to seed=1, chains=4, iter=20000, warmup=5000, and thin=4. If convergence was not attained, adjustments were made to iter=25000 and warmup=10000, ensuring *R*hat values remained below 1.10.

Prior Distributions: Uniformly set to Gaussian.

Model details: Comprehensive details including the response variable, predictors, random effects, and estimation results are available in the supplementary table#. Results included posterior median estimates, Bayesian 95% credible intervals, and approximate *p*-values (*p*MCMC) computed from posterior sampling.

Posterior sampling and *p*MCMC calculation: To test whether the posterior distribution of the difference in each treatment was above or below 0, we followed references[81–84]. Posterior samplings of each parameter were stored in diff_samples, and pairwise comparisons of treatments were made using the formula: *p*MCMC = 2 * min(mean(diff_samples > 0), mean(diff_samples < 0)).

Correlation analysis

The Pearson correlation coefficient and confidence intervals were computed using the pearsonr function from the scipy.stats library.

References

1. Spitschan, M., Aguirre, G. K., Brainard, D. H. & Sweeney, A. M. Variation of outdoor illumination as a function of solar elevation and light pollution. *Sci. Rep.* **6**, 26756 (2016).
   DOI: 10.1038/srep26756
2. Song, B. M. & Lee, C. H. Toward a mechanistic understanding of color vision in insects. *Front. Neural Circuits* **12**, 16 (2018).
   DOI: 10.3389/fncir.2018.00016
3. Numata, H., Miyazaki, Y. & Ikeno, T. Common features in diverse insect clocks. *Zoological Lett.* **1**, 10 (2015).
   DOI: 10.1186/s40851-014-0003-y
4. Kavakli, I. H., Ozturk, N. & Gul, S. DNA repair by photolyases. *Adv Protein. Chem. Struct. Biol.* **115**, 1–19 (2019).
   DOI: 10.1016/bs.apcsb.2018.10.003
5. Shibuya, K., Onodera, S. & Hori, M. Toxic wavelength of blue light changes as insects grow. *PLoS One* **13**, e0199266 (2018).
   DOI: 10.1371/journal.pone.0199266
6. Hori, M., Shibuya, K., Sato, M. & Saito, Y. Lethal effects of short-wavelength visible light on insects. *Sci. Rep.* **4**, 7383 (2014).
   DOI: 10.1038/srep07383
7. Hori, M. & Suzuki, A. Lethal effect of blue light on strawberry leaf beetle, Galerucella grisescens (Coleoptera: Chrysomelidae). *Sci. Rep.* **7**, 2694 (2017).
   DOI: 10.1038/s41598-017-03017-z
8. Nash, T. R., Chow, E. S., Law, A. D., Fu, S. D., Fuszara, E., Bilska, A., Bebas, P., Kretzschmar, D & Giebultowicz, J. M. Daily blue-light exposure shortens lifespan and causes brain neurodegeneration in *Drosophila*. *npj Aging Mech. Dis.* **5**, 8 (2019).
   DOI: 10.1038/s41514-019-0038-6
9. Hall, H., Ma, J., Shekhar, S., Leon-Salas, W. D. & Weake, V. M. Blue light induces a

736 neuroprotective gene expression program in *Drosophila* photoreceptors. *BMC*
737 *Neurosci.* **19**, 43 (2018).
738 DOI: 10.1186/s12868-018-0443-y
739 10. Yang, J., Song, Y., Law, A. D., Rogan, C. J., Shimoda, K., Djukovic, D., Anderson, J.
740 C., Hendrix, D. A & Giebultowicz, J. M. Chronic blue light leads to accelerated aging
741 in *Drosophila* by impairing energy metabolism and neurotransmitter levels. *Front.*
742 *Aging* **3**, 983373 (2022).
743 DOI: 10.3389/fragi.2022.983373
744 11. Song, Y., Yang, J., Law, A. D., Hendrix, D. A., Kretzschmar, D., Robinson, M &
745 Giebultowicz, J. M. Age-dependent effects of blue light exposure on lifespan,
746 neurodegeneration, and mitochondria physiology in *Drosophila melanogaster*. *npj*
747 *Aging* **8**, 11 (2022).
748 DOI: 10.1038/s41514-022-00092-z
749 12. Stanhope, S. C., Brandwine-Shemmer, T., Blum, H. R., Doud, E. H., Jannasch, A.,
750 Mosley, A. L., Minke, B & Weake, V. M. Proteome-wide quantitative analysis of redox
751 cysteine availability in the *Drosophila melanogaster* eye reveals oxidation of
752 phototransduction machinery during blue light exposure and age. *Redox Biol.* **63**,
753 102723 (2023).
754 DOI: 10.1016/j.redox.2023.102723
755 13. Scheiner, S. M. Selection experiments and the study of phenotypic plasticity. *J Evol.*
756 *Biol.* **15**, 889–898 (2002).
757 DOI: 10.1046/j.1420-9101.2002.00468.x
758 14. Martínez, A. A. & Lang, G. I. Identifying targets of selection in laboratory evolution
759 experiments. *J. Mol. Evol.* **91**, 345–355 (2023).
760 DOI: 10.1007/s00239-023-10096-2
761 15. Harshman, L. G. & Hoffmann, A. A. Laboratory selection experiments using
762 *Drosophila*: what do they really tell us? *Trends Ecol. Evol.* **15**, 32-36 (2000).
763 DOI: 10.1016/S0169-5347(99)01756-5

764 16. Watson, M. J. O. & Hoffmann, A. A. Acclimation, cross-generation effects, and the
765 response to selection for increased cold resistance in *Drosophila*. *Evolution* **50**, 1182-
766 1192 (1996).
767 DOI: 10.1111/j.1558-5646.1996.tb02359.x
768 17. Sørensen, J. G., Schou, M. F. & Loeschcke, V. Evolutionary adaptation to
769 environmental stressors: a common response at the proteomic level. *Evolution* **71**,
770 1627–1642 (2017).
771 DOI: 10.1111/evo.13243
772 18. Bastide, H., Yassin, A., Johanning, E. J. & Pool, J. E. Pigmentation in *Drosophila*
773 melanogaster reaches its maximum in Ethiopia and correlates most strongly with ultra-
774 violet radiation in sub-Saharan Africa. *BMC Evol. Biol.* **14**, 179 (2014).
775 DOI: 10.1186/s12862-014-0179-y
776 19. Akhmetova, K., Balasov, M. & Chesnokov, I. *Drosophila* STING protein has a role in
777 lipid metabolism. *eLife* **10**, e67358 (2021).
778 DOI: 10.7554/eLife.67358
779 20. Bailey, A. P., Koster, G., Guillermier, C., Hirst, E. M. A., MacRae, J. I., Lechene, C. P.,
780 Postle, A. D & Gould, A. P. Antioxidant role for lipid droplets in a stem cell niche of
781 *Drosophila*. *Cell* **163**, 340–353 (2015).
782 DOI: 10.1016/j.cell.2015.09.020
783 21. Moulton, M. J., Barish, S., Ralhan, I., Chang, J., Goodman, L., Harland, J. G.,
784 Marcogliese, P. C., Johansson, J. O., Ioannou, M. S. & Bellen, H. J. Neuronal ROS-
785 induced glial lipid droplet formation is altered by loss of Alzheimer's disease-
786 associated genes. *Proc. Natl. Acad. Sci. UAS* **118**, e2112095118 (2021).
787 DOI: 10.1073/pnas.2112095118
788 22. Zhao, S., Jang, C., Liu, J., Uehara, K., Gilbert, M., Izzo, L., Zeng, X., Trefely, S.,
789 Fernandez, S., Carrer, A., Miller, K. D., Schug, Z. T., Snyder, N. W., Gade, T. P.,
790 Rabinowitz, J. D. & Wellen, K. E. Dietary fructose feeds hepatic lipogenesis via
791 microbiota-derived acetate. *Nature* **579**, 586–591 (2020).

792 DOI: 10.1038/s41586-020-2101-7
793 23. Jugder, B. E., Kamareddine, L. & Watnick, P. I. Microbiota-derived acetate activates
794 intestinal innate immunity via the Tip60 histone acetyltransferase complex. *Immunity*
795 **54**, 1683-1697.e3 (2021).
796 DOI: 10.1016/j.immuni.2021.05.017
797 24. Paiva, P., Medina, F. E., Viegas, M., Ferreira, P., Neves, R. P. P., Sousa, J. P. M.,
798 Ramos, M. J. & Fernandes, P. A. Animal fatty acid synthase: a chemical nanofactory.
799 *Chem. Rev.* **121**, 9502–9553 (2021).
800 DOI: 10.1021/acs.chemrev.1c00147
801 25. Miao, T., Kim, J., kang, P., Fujiwara, H., Hsu, FF & Bai, H. Acetyl-CoA-mediated
802 autoacetylation of fatty acid synthase as a metabolic switch of de novo lipogenesis in
803 *Drosophila*. *Proc. Natl. Acad. Sci. USA* **119**, e2212220119 (2022).
804 DOI: 10.1073/pnas.2212220119
805 26. Onuma, T., Yamauchi, T., Kosakamoto, H., Kadoguchi, H., Kuraishi, T., Murakami, T.,
806 Mori, H., Miura, M. & Obata, F. Recognition of commensal bacterial peptidoglycans
807 defines *Drosophila* gut homeostasis and lifespan. *PLoS Genet.* **19**, e1010709 (2023).
808 DOI: 10.1371/journal.pgen.1010709
809 27. Chaston, J. M., Newell, P. D. & Douglas, A. E. Metagenome-wide association of
810 microbial determinants of host phenotype in *Drosophila melanogaster*. *mBio* **5**,
811 e01631-14 (2014).
812 DOI: 10.1128/mbio.01631-14
813 28. Newell, P. D. & Douglas, A. E. Interspecies interactions determine the impact of the
814 gut microbiota on nutrient allocation in *Drosophila melanogaster*. *Appl. Environ.*
815 *Microbiol.* **80**, 788–796 (2014).
816 DOI: 10.1128/AEM.02742-13
817 29. He, Y., Xie, Z., Zhang, H., Liebl, W., Toyama, H. & Chen, F. Oxidative fermentation of
818 acetic acid bacteria and its products. *Front. Microbiol.* **13**, 879246 (2022).
819 DOI: 10.3389/fmicb.2022.879246

30. Shin, S. C., Kim, SH., You, H., Kim, B., Kim, A. C., Lee, KA., Yoon, JH., Ryu, JH. &Lee, WJ. *Drosophila* microbiome modulates host developmental and metabolic homeostasis via insulin signaling. *Science* **334**, 670–674 (2011).
DOI: 10.1126/science.1212782

31. Chaston, J. M., Dobson, A. J., Newell, P. D. & Douglas, A. E. Host genetic control of the microbiota mediates the *Drosophila* nutritional phenotype. *Appl. Environ. Microbiol.* **82**, 671–679 (2016).
DOI: 10.1128/AEM.03301-15

32. Gould, A. L., Zhang, V., Lamberti, L., Jones, E. W., Obadia, B., Korasidis, N., Gavryushkin, A., Carlson, J. M., Beerenwinkel, N. & Ludington, W. B. Microbiome interactions shape host fitness. *Proc. Natl. Acad. Sci. USA* **115**, E11951-E11960 (2018).
DOI: 10.1073/pnas.1809349115

33. Elgart, M., Stern, S., Salton, O., Gnainsky, Y., Heifetz, Y. & Soen, Y. Impact of gut microbiota on the fly's germ line. *Nat. Commun.* **7**, 11280 (2016).
DOI: https://doi.org/10.1038/ncomms11280

34. Henriques, S. F., Dhakan, D. B., Serra, L., Francisco, A. P., Carvalho-Santos, Z., Baltazar, C., Elias, A. P., Anjos, M., Zhang, T., Maddocks, O. D. K. & Ribeiro, C. Metabolic cross-feeding in imbalanced diets allows gut microbes to improve reproduction and alter host behaviour. *Nat. Commun.* **11**, 4236 (2020).
DOI: 10.1038/s41467-020-18049-9

35. Dodge, R., Jones, E. W., Zhu, H., Obadia, B., Martinez, D. J., Wang, C., Aranda-Díaz, A., Aumiller, K., Liu, Z., Voltolini, M., Brodie, E. L., Huang, K. C., Carlson, J. M., Sivak, D. A., Spradling, A. C. & Ludington, W. B. A symbiotic physical niche in *Drosophila melanogaster* regulates stable association of a multi-species gut microbiota. *Nat. Commun.* **14**, 1557 (2023).
DOI: 10.1038/s41467-023-36942-x

36. Broderick, N. A., Buchon, N. & Lemaitre, B. Microbiota-induced changes in *Drosophila*

848 *melanogaster* host gene expression and gut morphology. *mBio* **5**, e01117-14 (2014).
849 DOI: 10.1128/mBio.01117-14
850 37. Yu, FX., Zhao, B. & Guan, KL. Hippo pathway in organ size control, tissue
851 homeostasis, and cancer. *Cell* **163**, 811–828 (2015).
852 DOI: 10.1016/j.cell.2015.10.044
853 38. Li, Q., Nirala, N. K., Nie, Y., Chen, HJ., Ostroff, G., Mao, J., Wang, Q., Xu, L. & Ip, Y.
854 T. Ingestion of food particles regulates the mechanosensing Misshapen-Yorkie
855 pathway in *Drosophila* intestinal growth. *Dev. Cell* **45**, 433-449.e6 (2018).
856 DOI: 10.1016/j.devcel.2018.04.014
857 39. Huang, HL., Wang, S., Yin, MX., Dong, L., Wang, C., Lu, Y., Feng, M., Dai, C., Guo,
858 X., Li, L., Zhao, B., Zhou, Z., Ji, H., Jiang, J., Zhao, Y., Liu, XY. & Zhang, L. Par-1
859 regulates tissue growth by influencing Hippo phosphorylation status and Hippo-
860 Salvador association. *PLoS Biol.* **11**, e1001620 (2013).
861 DOI: 10.1371/journal.pbio.1001620
862 40. Li, Q., Li, S., Mana-Capelli, S., Flach, R. J. R., Danai, L. V., Amcheslavsky, A., Nie, Y.,
863 Kaneko, S., Yao, X., Chen, X., Cotton, J. L., Mao, J., McCollum, D., Jiang, J., Czech,
864 M. P., Xu, L. & Ip, Y. T. The conserved Misshapen-Warts-Yorkie pathway acts in
865 enteroblasts to regulate intestinal stem cells in *Drosophila*. *Dev. Cell* **31**, 291–304
866 (2014).
867 DOI: 10.1016/j.devcel.2014.09.012
868 41. Nyholm, L., Koziol, A., Marcos, S., Botnen, A. B., Aizpurua, O., Gopalakrishnan, S.,
869 Limborg, M. T., Gilbert, M. T. P. & Alberdi, A. Holo-omics: integrated host-microbiota
870 multi-omics for basic and applied biological research. *iScience* **23**, 101414 (2020).
871 DOI: 10.1016/j.isci.2020.101414
872 42. Moschandrea, C., Kondylis, V., Evangelakos, I., Herholz, M., Schneider, F., Schmidt,
873 C., Yang, M., Ehret, S., Heine, M., Jaeckstein, M. Y., Szczepanowska, K., Schwarzer,
874 R., Baumann, L., Bock, T., Nikitopoulou, E., Brodesser, S., Krüger, M., Frezza, C.,
875 Heeren, J., Trifunovic, A. & Pasparakis, M. Mitochondrial dysfunction abrogates

876 dietary lipid processing in enterocytes. *Nature* **625**, 385–392 (2024).
877 DOI: 10.1038/s41586-023-06857-0
878 43. Byrns, C. N., Perlegos, A. E., Miller, K. N., Jin, Z., Carranza, F. R., Manchandra, P.,
879 Beveridge, C. H., Randolph, C. E., Chaluvadi, V. S., Zhang, S. L., Srinivasan, A. R.,
880 Bennett, F. C., Sehgal, A., Adams, P. D., Chopra, G. & Bonini, N. M. Senescent glia
881 link mitochondrial dysfunction and lipid accumulation. *Nature* **630**, 475–483 (2024).
882 DOI: 10.1038/s41586-024-07516-8
883 44. Chatterjee, N. & Perrimon, N. What fuels the fly: energy metabolism in *Drosophila* and
884 its application to the study of obesity and diabetes. *Sci. Adv.* **7**, eabg4336 (2021).
885 DOI: 10.1126/sciadv.abg433
886 45. Heier, C. & Kühnlein, R. P. Triacylglycerol metabolism in *Drosophila melanogaster*.
887 *Genetics* **210**, 1163–1184 (2018).
888 DOI: 10.1534/genetics.118.301583
889 46. Song, W., Veenstra, J. A. & Perrimon, N. Control of lipid metabolism by Tachykinin in
890 *Drosophila*. *Cell Rep.* **9**, 40–47 (2014).
891 DOI: 10.1016/j.celrep.2014.08.060
892 47. Kamareddine, L., Robins, W. P., Berkey, C. D., Mekalanos, J. J. & Watnick, P. I. The
893 *Drosophila* immune deficiency pathway modulates enteroendocrine function and host
894 metabolism. *Cell Metab.* **28**, 449-462.e5 (2018).
895 DOI: 10.1016/j.cmet.2018.05.026
896 48. Henry, L. P., Bruijning, M., Forsberg, S. K. G. & Ayroles, J. F. The microbiome extends
897 host evolutionary potential. *Nat. Commun.* **12**, 5141 (2021).
898 DOI: 10.1038/s41467-021-25315-x
899 49. Henry, L. P. & Ayroles, J. F. Meta-analysis suggests the microbiome responds to
900 evolve and resequence experiments in *Drosophila melanogaster*. *BMC Microbiol.* **21**,
901 108 (2021).
902 DOI: 10.1186/s12866-021-02168-4
903 50. Bruijning, M., Henry, L. P., Forsberg, S. K. G., Metcalf, C. J. E. & Ayroles, J. F. Natural

904 selection for imprecise vertical transmission in host–microbiota systems. *Nat. Ecol.*
905 *Evol.* **6**, 77–87 (2022).
906 DOI: 10.1038/s41559-021-01593-y
907 51. Henry, L. P., Fernandez, M., Webb, A. & Ayroles, J. F. Host evolutionary history and
908 ecological context modulate the adaptive potential of the microbiome. Preprint at
909 https://doi.org/10.1101/2020.09.21.306779 (2020).
910 52. Liu, L., Zhang, K., Sandoval, H., Yamamoto, S., Jaiswal., M., Sanz, E., Li, Z., Hul, J.,
911 Graham, B. H., Quintana, A. & Bellen, H. J. Glial lipid droplets and ROS induced by
912 mitochondrial defects promote neurodegeneration. *Cell* **160**, 177–190 (2015).
913 DOI: 10.1016/j.cell.2014.12.019
914 53. Reiff, T., Jacobson, J., Cognigni, P., Antonello, Z., Ballesta, E., Junn, Tan, K. J., Yew,
915 J. Y., Dominguez, M. & Miguel-Aliaga, I. Endocrine remodelling of the adult intestine
916 sustains reproduction in *Drosophila. eLife* **4**, e06930 (2015).
917 DOI: 10.7554/eLife.06930
918 54. Buszczak, M., Lu, X., Segraves, W. A., Chang, T. Y. & Cooley, L. Mutations in the
919 Midway gene disrupt a *Drosophila* Acyl Coenzyme A: diacylglycerol acyltransferase.
920 *Genetics* **160**, 1511-1518 (2002).
921 DOI: 10.1093/genetics/160.4.1511
922 55. Murphy, M. P. How mitochondria produce reactive oxygen species. *Biochem. J.* **417**,
923 1–13 (2009).
924 DOI: 10.1042/BJ20081386
925 56. Crotti, E., Rizzi, A., Chouaia, B., Ricci, I., Favia, G., Alma, A., Sacchi, L., Bourtzis, K.,
926 Mandrioli, M., Cherif, A., Bandi, C. & Daffonchio, D. Acetic acid bacteria, newly
927 emerging symbionts of insects. *Appl. Environ. Microbiol.* **76**, 6963–6970 (2010).
928 DOI: 10.1128/AEM.01336-10
929 57. Shi, L. & Tu, B. P. Acetyl-CoA and the regulation of metabolism: mechanisms and
930 consequences. *Curr. Opin. Cell Biol.* **33**, 125–131 (2015).
931 DOI: 10.1016/j.ceb.2015.02.003

58. Li, X. & Karpac, J. A distinct Acyl-CoA binding protein (ACBP6) shapes tissue plasticity during nutrient adaptation in *Drosophila*. *Nat. Commun.* **14**, 7599 (2023). DOI: 10.1038/s41467-023-43362-4

59. Narita, T., Weinert, B. T. & Choudhary, C. Functions and mechanisms of non-histone protein acetylation. *Nat. Rev. Mol. Cell Biol.* **20**, 156-174 (2019). DOI: 10.1038/s41580-018-0081-3

60. Christensen, C. F., Laurichesse, Q., Loudhaief, R., Colombani, J. & Andersen, D. S. *Drosophila* activins adapt gut size to food intake and promote regenerative growth. *Nat. Commun.* **15**, 273 (2024). DOI: 10.1038/s41467-023-44553-9

61. Nagai, H., Nagai, L. A. E., Tasaki, S., Nakato, R, Umetsu, D., Kuranaga, E., Miura, M. & Nakajima, Y. Nutrient-driven dedifferentiation of enteroendocrine cells promotes adaptive intestinal growth in *Drosophila*. *Dev. Cell* **58**, 1764-1781.e10 (2023). DOI: 10.1016/j.devcel.2023.08.022

62. Karasov, W. H., Martínez Del Rio, C. & Caviedes-Vidal, E. Ecological physiology of diet and digestive systems. *Annu. Rev. Physiol.* **73**, 69–93 (2011). DOI: 10.1146/annurev-physiol-012110-142152

63. Stojanović, O., Miguel-Aliaga, I. & Trajkovski, M. Intestinal plasticity and metabolism as regulators of organismal energy homeostasis. *Nat. Metab.* **4**, 1444–1458 (2022). DOI: 10.1038/s42255-022-00679-6

64. Miguel-Aliaga, I., Jasper, H. & Lemaitre, B. Anatomy and physiology of the digestive tract of *Drosophila melanogaster*. *Genetics* **210**, 357–396 (2018). DOI: 10.1534/genetics.118.300224

65. Chevalier, C., Stojanović, O., Colin, D. J., Suarez-Zamorano, N., Tarallo, V., Veyrat-Durebex, C., Rigo, D., Fabbiano, S., Stevanović, A., Hagemann, S., Montet, X., Seimbille, Y., Zamboni, N., Hapfelmeier, S. & Trajkovski, M. Gut microbiota orchestrates energy homeostasis during cold. *Cell* **163**, 1360–1374 (2015). DOI: 10.1016/j.cell.2015.11.004

960 66. Buchon, N., Osman, D., David, F. P. A., Fang, H. Y., Boquete, JP., Deplancke, B. &
961 Lemaitre, B. Morphological and molecular characterization of adult midgut
962 compartmentalization in *Drosophila*. *Cell Rep.* **3**, 1725–1738 (2013).
963 DOI: 10.1016/j.celrep.2013.04.001
964 67. Fitz-James, M. H. & Cavalli, G. Molecular mechanisms of transgenerational epigenetic
965 inheritance. *Nat. Rev. Genet.* **23**, 325–341 (2022).
966 DOI: 10.1038/s41576-021-00438-5
967 68. Huang, J., Zhou, F., Zhou, H., Zheng, X., Huo, Z., Yang, M., Xu, Z., Liu, R., Wang, L.
968 & Wang, X. Systematic assessment of transcriptomic and metabolic reprogramming
969 by blue light exposure coupled with aging. *PNAS Nexus* **2**, 1-15(2023).
970 DOI: 10.1093/pnasnexus/pgad390
971 69. Torquato, L. S., Mattos, D., Matta, B. P. & Bitner-Mathé, B. C. Cellular basis of
972 morphological variation and temperature-related plasticity in *Drosophila melanogaster*
973 strains with divergent wing shapes. *Genetica* **142**, 495–505 (2014).
974 DOI: 10.1007/s10709-014-9795-0
975 70. Lee, J. H., Bassel-Duby, R. & Olson, E. N. Heart- and muscle-derived signaling system
976 dependent on MED13 and Wingless controls obesity in *Drosophila*. *Proc. Natl. Acad.*
977 *Sci. USA* **111**, 9491–9496 (2014).
978 DOI: 10.1073/pnas.1409427111
979 71. Bligh. E. G & Dyer. W. J. A rapid method of total lipid extraction and purification. *Can.*
980 *J. Biochem. Physiol.* **37**, 911-7 (1959).
981 DOI: 10.1139/o59-099
982 72. Guan, X. L., Cestra, G., Shui, G., Kuhrs, A., Schittenhelm, R. B., Hafen, E., van der
983 Goot, F. G., Robinett, C. C., Gatti, M., Gonzalez-Gaitan, M. & Wenk, M. R. Biochemical
984 membrane lipidomics during *Drosophila* development. *Dev. Cell* **24**, 98–111 (2013).
985 DOI: 10.1016/j.devcel.2012.11.012
986 73. Shen, L. R., Lai, C. Q., Feng, X., Parnell, L. D., Wan, J. B., Wang, J. D., Li, D., Ordovas,
987 J. M. & Kang, J. X. *Drosophila* lacks C20 and C22 PUFAs. *J. Lipid Res.* **51**, 2985–

988 2992 (2010).
989 DOI: 10.1194/jlr.M008524
990 74. Wood, J. G., Schwer, B., Wickremesinghe, P. C., Hartnett, D. A., Garcia, M., Li, M.,
991 Verdin, E. & Helfand, S. L. Sirt4 is a mitochondrial regulator of metabolism and lifespan
992 in *Drosophila melanogaster*. *Proc. Natl. Acad. Sci. USA* **115**, 1564–1569 (2018).
993 DOI: 10.1073/pnas.172067311
994 75. Ward, J. H. Hierarchical grouping to optimize an objective function. *J. Am. Stat. Assoc.*
995 **58**, 236-244 (1963).
996 DOI: 10.1080/01621459.1963.10500845
997 76. Weisburg, W. G., Barns, S. M., Pelletier, D. A. & Lane, D. J. 16S Ribosomal DNA
998 amplification for phylogenetic study. *J. Bacteriol.* **173**, 697-703 (1991).
999 DOI: 10.1128/jb.173.2.697-703.1991
1000 77. Edwards, U., Rogall, T., Blöcker, H., Emde, M. & Böttger, E. C. Isolation and Direct
1001 Complete Nucleotide Determination of Entire Genes. Characterization of a Gene
1002 Coding for 16S Ribosoma] RNA. *Nucleic Acids Res.* **17**, 7843-7853 (1989).
1003 DOI: 10.1093/nar/17.19.7843
1004 78. Leftwich, P. T., Clarke, N. V. E., I. Hutchings, M. & Chapman, T. Gut microbiomes and
1005 reproductive isolation in *Drosophila*. *Proc. Natl. Acad. Sci. USA* **114**, 12767-12772
1006 (2017).
1007 DOI: 10.1073/pnas.1708345114
1008 79. Kanno, M., Hiramatsu, S., Kondo, S., Tanimoto, H. & Ichinose, T. Voluntary intake of
1009 psychoactive substances is regulated by the dopamine receptor Dop1R1 in
1010 *Drosophila*. *Sci. Rep*. **11**, 3432 (2021).
1011 DOI: 10.1038/s41598-021-82813-0
1012 80. Wierzbicki, F., Schwarz, F., Cannalonga, O. & Kofler, R. Novel quality metrics allow
1013 identifying and generating high-quality assemblies of piRNA clusters. *Mol. Ecol.*
1014 *Resour.* **22**, 102–121 (2022).
1015 DOI: 10.1111/1755-0998.13455

81. Bürkner, P. C. brms: An R package for Bayesian multilevel models using Stan. *J. Stat. Softw.* **80**, 1-28 (2017).
DOI: 10.18637/jss.v080.i01

82. Nott, D. J., Drovandi, C. C., Mengersen, K. & Evans, M. Approximation of Bayesian predictive *p*-values with regression ABC. *Bayesian Anal.* **13**, 59–83 (2018).
DOI: 10.1214/16-BA1033

83. Cornwallis, C. K., van't Padje, A., Ellers, J., Klein, M., Jackson, R., Kiers, E. T., West, S. A. & Henry L. M. Symbioses shape feeding niches and diversification across insects. *Nat. Ecol. Evol.* **7**, 1022–1044 (2023).
DOI: 10.1038/s41559-023-02058-0

84. Hadfield, J. D. MCMC methods for multi-response generalized linear mixed models: The MCMCglmm R package. *J. Stat. Softw.* **33**, 1-22 (2010).
DOI: 10.18637/jss.v033.i02

Acknowledgements

We are grateful to Dr. Takema Fukatu, Dr. Yuto Yoshinari, Dr. Takashi Nishimura, and Dr. Koichiro Tamura for their valuable discussions regarding the study. We also thank Dr. Masaki Iwata, Dr. Shuhei Miyashita, Dr. Chisato Kobayashi, Dr. Yuma Takahashi, Dr. Takahisa Ueno, Dr. Masashi Murakami and Dr. Sota Tanaka for their important suggestions. We would like to thank Dr. Atsuhiko Nagasawa and Mr Yuki Chiba for teaching us the GC/MS-MS analysis, and Dr. Fu Namai for teaching us about microbiome analysis. We also thank Mr. Yusaku Hayashi for instructing us on how to dissect the fat body. Ms. Ayako Abe and Mr. Kento Fukuoka provided technical assistance. We extend our gratitude to Dr. Haruki Kitazawa and Dr. Shoichiro Kurata for lending us their laboratories. We thank the Rhelixa, Inc, Bloomington Drosophila Stock Center and Japan Collection of Microorganisms RIKEN BioResource Research Center.

This work was supported by JST SPRING, Grant Number JPMJSP2102.

Author information

Authors and Affiliations

Graduate School of Agricultural Sciences, Tohoku University, Sendai, Japan

Yuta Takada, Wakako Ikeda-Ohtsubo and Masatoshi Hori

Frontier Research Institute for Interdisciplinary Sciences, Tohoku University, Sendai, Japan

Toshiharu Ichinose

Graduate School of Pharmaceutical Sciences, Tohoku University, Sendai, Japan

Naoyuki Fuse

Graduate School of Life Sciences, Tohoku University, Sendai, Japan

Toshiharu Ichinose, Kokoro Saito and Hiromu Tanimoto

Contributions

Y.T. and M.H. conceived and designed d the study. Y.T. performed all experiments and analyzed all data, wrote the original manuscript, edited the first manuscript, and reviewed and edited the second manuscript. Y.T. and W.I. designed and performed the infection experiment with gut contents and bacterial experiments. Y.T., T.I., and N.F. performed and analyzed whole genome sequencing and RNA-sequencing. Y.T., K.S., T.I., and H.T. designed the genetics and CAFE assay. Y.T. and K.S. performed the CAFE assay. W.I., N.F., and T.I. edited the first manuscript. H.T. and M.H. supervised the study. All authors participated in the discussion and reviewed the final manuscript.

Figures

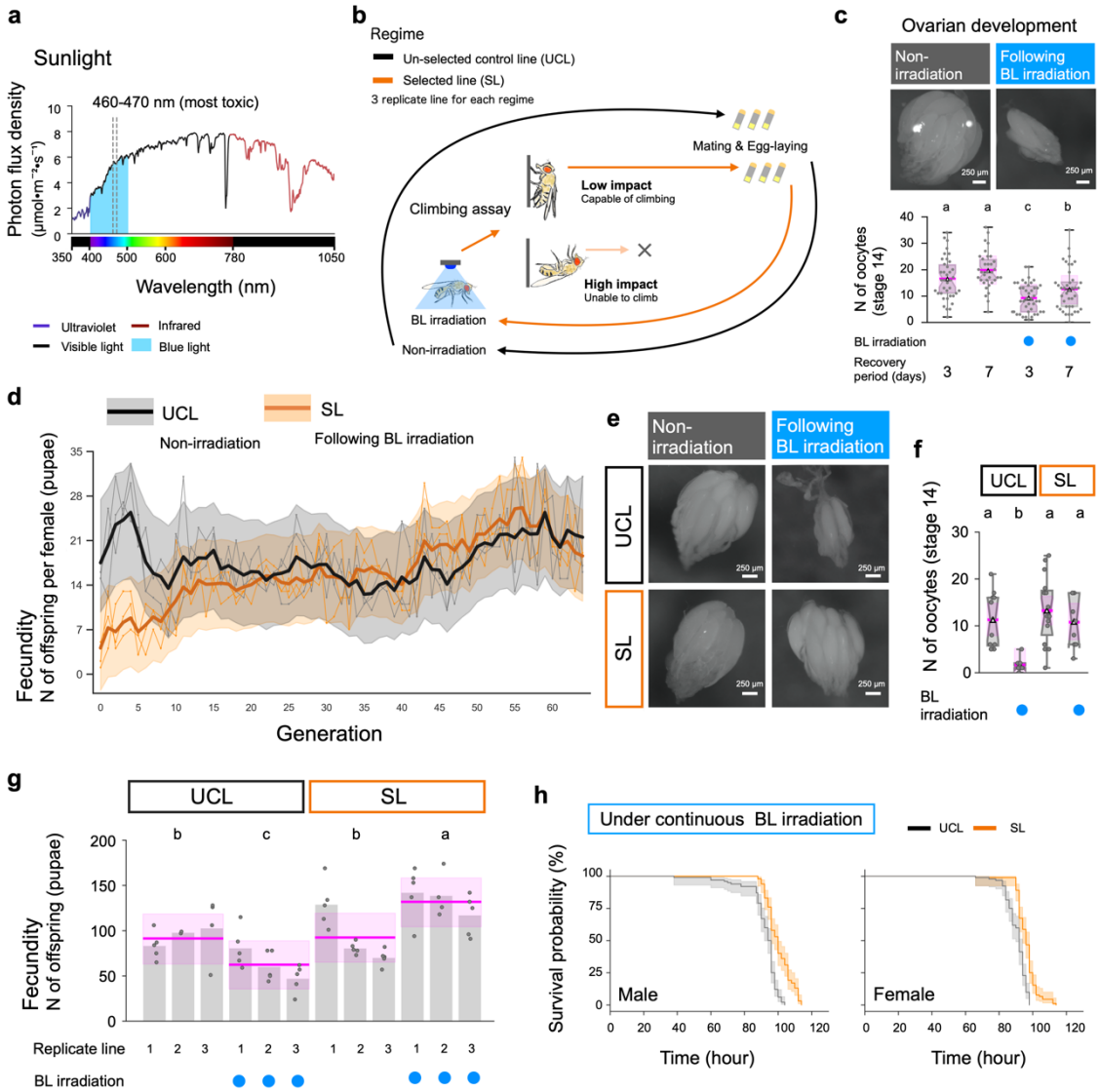

Fig. 1 | Establishment of *Drosophila* lines with blue light (BL)-tolerance evolved by laboratory selection

a, Sunlight conditions. Photon flux density: 4,050 μmol·m^{-2}·s^{-1} (BL (400-500 nm): 471 μmol·m^{-2}·s^{-1}). 460-470 nm is the most toxic wavelength range for *Drosophila* adults. **b**, Experimental design of laboratory selection using BL toxicity. After 3 days of BL irradiation and a 2-day recovery period, a climbing assay was performed. Flies capable of climbing were classified as "low impact", while those unable to climb were classified as "high impact". In the selected line (SL), "low impact" flies were allowed 5 days for mating

1080 and egg-laying. Unselected control line (UCL) parents were randomly chosen from the
1081 negative control group and reared under the same conditions as the SL flies. (for details,
1082 see "Laboratory selection for BL-tolerance" in Methods). **c**, Impact of BL toxicity on ovarian
1083 development. Number of stage 14 oocytes in virgin flies after different recovery periods.
1084 Gray: Non-irradiation; Blue: 3 days of BL irradiation. n = 34-42. BF_{10} > 100. (UCL,
1085 Generation 34). **d**, Changes in fecundity across generations resulting from laboratory
1086 selection. Fecundity measured as the number of offspring per female (pupae). n = 3.
1087 Bayesian state space model with Markov Chain Monte Carlo (MCMC) method, posterior
1088 median and Bayesian 95% Credible Intervals (CI). **e**, Ovarian development differences
1089 after 3 days of BL irradiation followed by 3 days of recovery. **f**, Number of stage 14 oocytes
1090 after a 3-day recovery period. n = 9-15. BF_{10} = 50.74. (Replicate line 2, Generation 25). **g**,
1091 Fecundity measured as the number of offspring (pupae). n = 11-15. BF_{10} = 50.74. Each plot
1092 involved the mating and egg-laying of 5 treated females and 5 untreated males for 4 days.
1093 (Generation 38). **h**, Lifespan under continuous BL irradiation. Top: male n = 100. BF_{10}
1094 >100. Estimates: UCL 90.62 h (89.38 to 91.82), SL 96.35 h (95.16 to 97.52), pMCMC <
1095 0.001. Bottom: female n = 92. BF_{10} = 0.72. Estimates: UCL 92.09 h (90.38 to 93.78), SL
1096 100.39 h (98.74 to 102.13), pMCMC < 0.001. (Replicate line 1, Generation 25).
1097 Statistical analyses for panels **b**-**h** used a Bayesian Hierarchical Model (HBM) with MCMC
1098 methods, posterior median, and Bayesian 95% Credible Intervals (CI). In **c**, **f** and **g**,
1099 significant differences between different letters indicate pMCMC < 0.05 (Supplementary
1100 Table 1).
1101

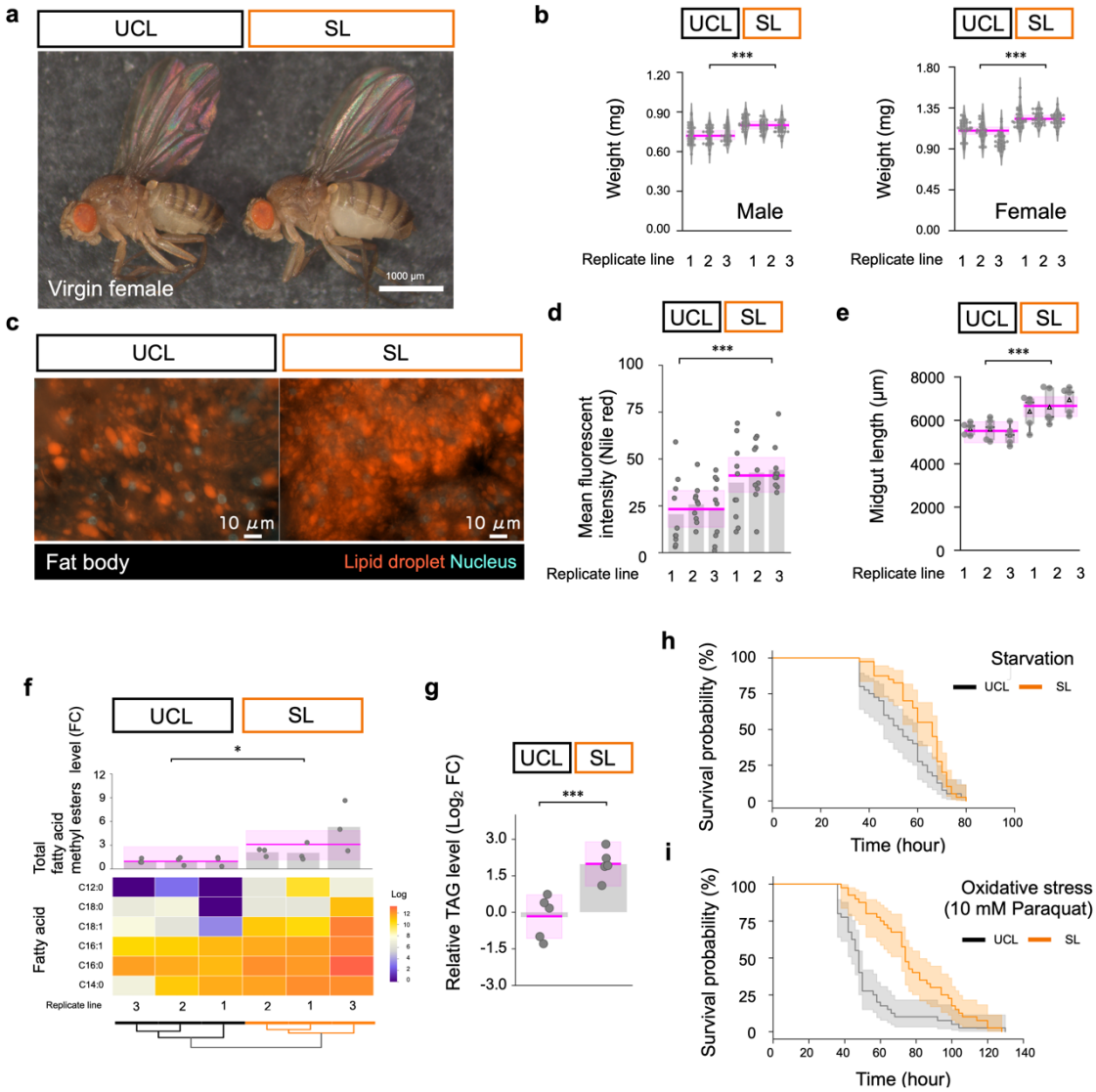

Fig. 2 | Selected line flies exhibited obese phenotype, lipid accumulation, and oxidative stress resistance.

a, Phenotype of adult virgin females aged 6-8 days: left, UCL; right, SL. **b**, Body weight, *n* = 90, BF_{10} >100, (Generation 39). **c**, Fluorescence imaging of abdominal fat body and lipid droplets (Lipid droplet: Nile red; Nucleus: NucBlue). **d**, Mean fluorescence intensity from Nile red staining, *n* = 30, BF_{10} >100, (Generation 35). **e**, Midgut length, *n* = 15, BF_{10} >100, (Generation 45). **f**, GC/MS analyses of Fatty Acid Methyl Esters (FAMEs), total FAMEs, *n* = 9, BF_{10} = 1.69 (Generation 30). **g**, Relative triacylglycerol (TAG) level, *n* = 5, BF_{10} =15.14, (Replicate line 1, Generation 57). **h**, Starvation resistance, Kaplan-Meier survival curve, *n* =

1112 40 , BF_{10} =4.49. Estimates: UCL 53.04 h (49.20 to 56.89), SL 61.91 h (58.09 to 65.43)
1113 (Replicate line 2, Generation 43). **i**, Oxidative stress resistance (10 mM paraquat), Kaplan-
1114 Meier survival curve, n = 40, BF_{10} >100. Estimates: UCL 53.07 h (45.90 to 59.03), SL 77.94
1115 h (71.19 to 84.08), (Replicate line 3, Generation 43). Statistical analyses for panels **b**, **d**, **e**,
1116 **f**, **g**, **h**, and **i** were performed using a HBM with MCMC methods, posterior median, and
1117 Bayesian 95% CI. Asterisks indicate significance levels: * pMCMC < 0.05, ** pMCMC < 0.01,
1118 *** pMCMC < 0.001. For details, see Supplementary Table 2 for all results, including
1119 statistical models.
1120

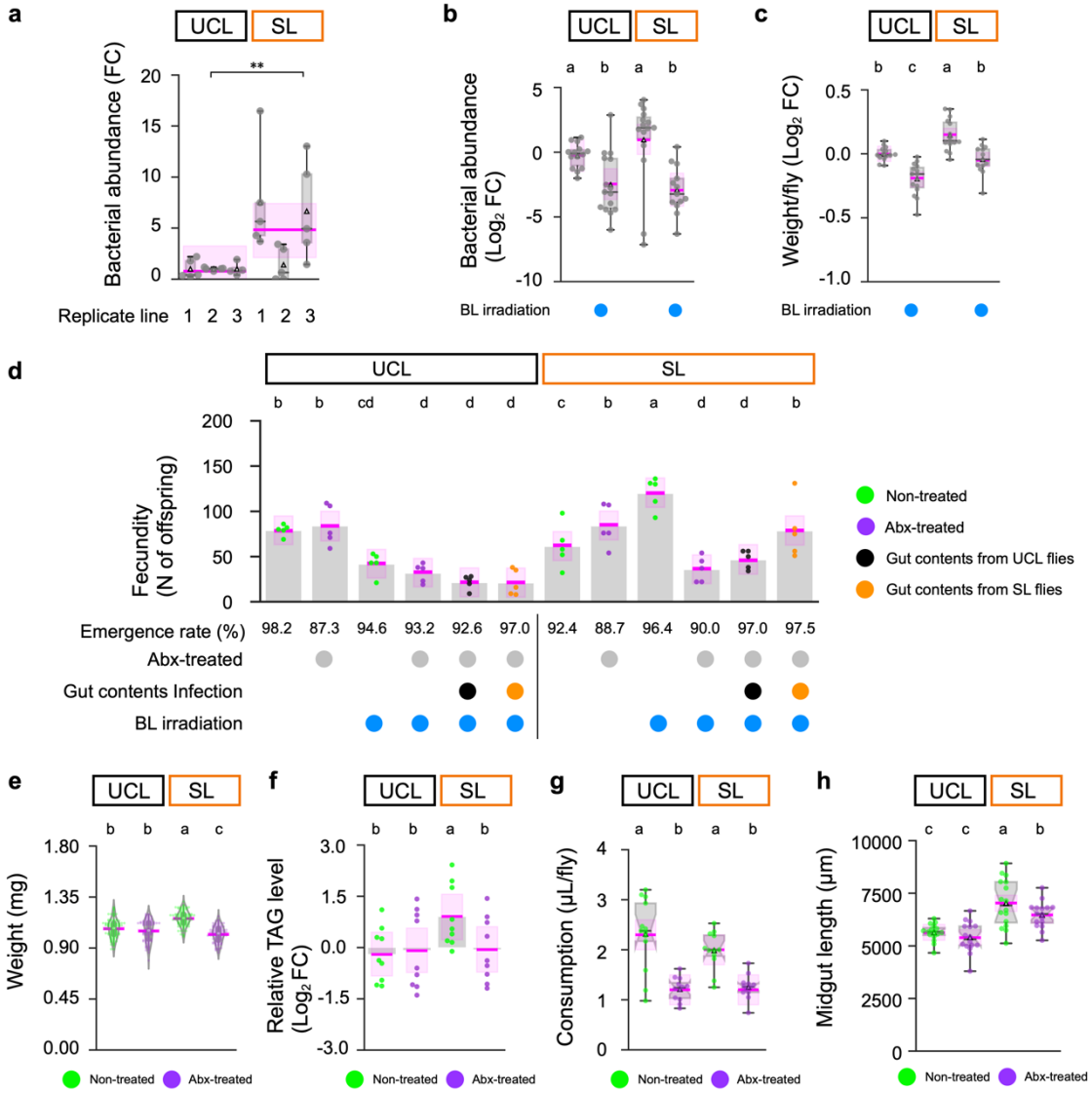

1121

1122 **Fig. 3 | High bacterial abundance is the key to BL-tolerance and lipid**

1123 **accumulation in SL flies.**

1124 **a,** Bacterial abundance, *n* = 15, BF_{10} = 9.22. Asterisks indicate significance: ** *p*MCMC <

1125 0.01. (Generation 38). **b**, Bacterial abundance, *n* = 13-15, BF_{10} >100. (Generation 38). **c**,

1126 Body weight, *n* = 16, BF_{10} >100. (Generation 38). **d,** Fecundity measured as the number of

1127 offspring (adults), *n* = 5, BF_{10} >100. (Replicate line 1, Generation 47) **e**, Body weight, *n* = 100,

1128 BF_{10} >100. (Replicate line 1, Generation 55). **f**, Relative TAG level, *n* = 10, BF10 = 1.47.

1129 (Replicate line 1, Generation 55). **g**, Food consumption, *n* = 12-13, BF_{10} >100. (Replicate

1130 line 1, Generation 52). **h,** Midgut length, n = 16, BF_{10} >100. (Replicate line 1, Generation 48).

Statistical analyses for panels **b**-**h** were performed using HBM with MCMC methods, posterior median, and Bayesian 95% CI. Significant differences between different letters indicate *p*MCMC < 0.05. For details, see Supplementary Table3 for all results, including statistical models.

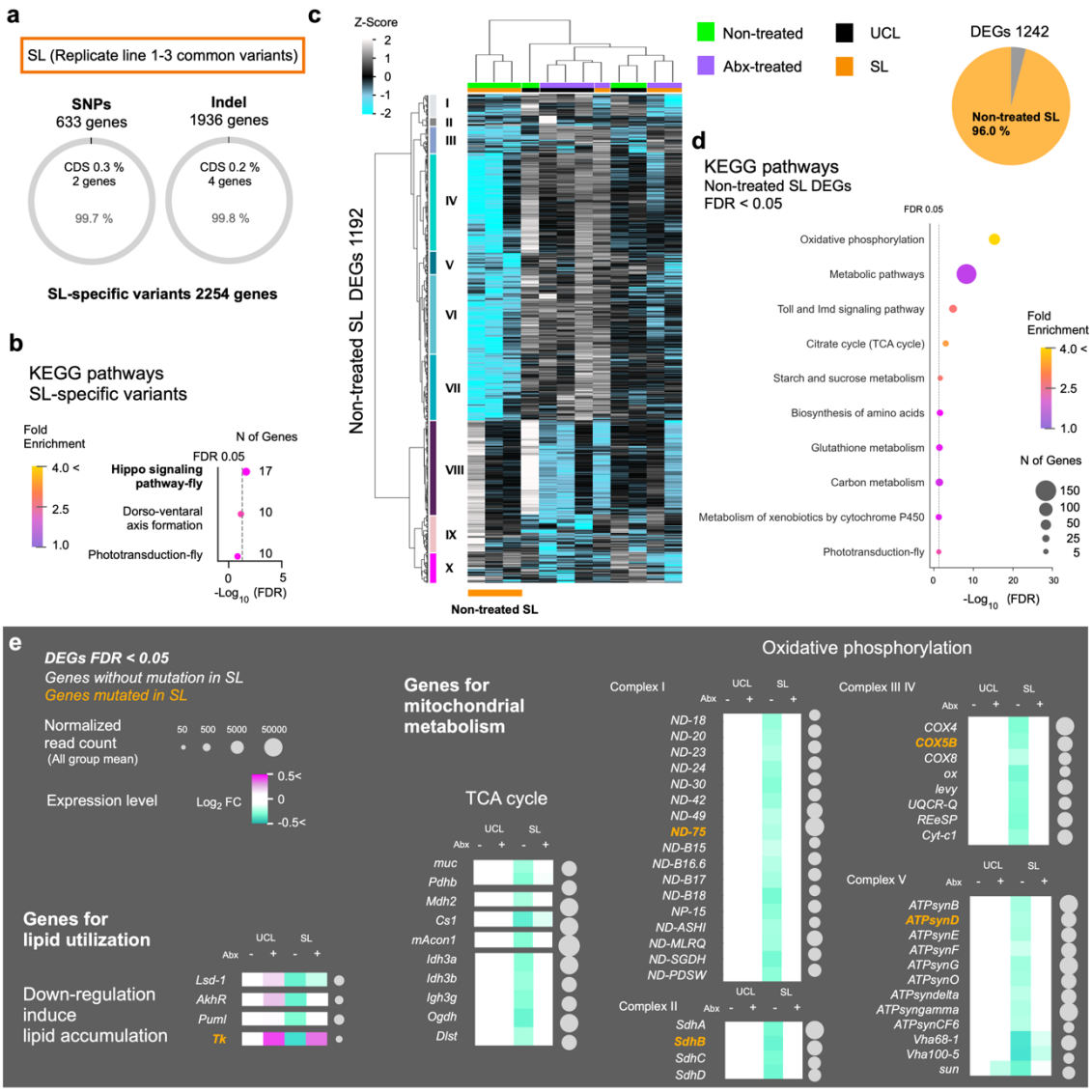

Fig. 4 | Host genome and transcriptomic profiles explain the characteristic phenotype of SL flies

a, Identification of SL-specific variants through whole genome resequencing (Generation 44). **b**, Enrichment analysis of SL-specific variants using Kyoto Encyclopedia of Genes and Genomes (KEGG) with an FDR-adjusted *p* value threshold of < 0.05. **c**, Cluster map of differentially expressed genes (DEGs) (Replicate line 1, Generation 50). **d**, Enrichment analysis of non-treated SL DEGs using KEGG with an FDR-adjusted *p* value threshold of < 0.05. **e**, Heatmaps illustrating functional profiles. All genes shown are DEGs (FDR < 0.05). Genes mutated in SL are indicated in orange.

1146 For details, see Supplementary Table 4 for all results.

1147

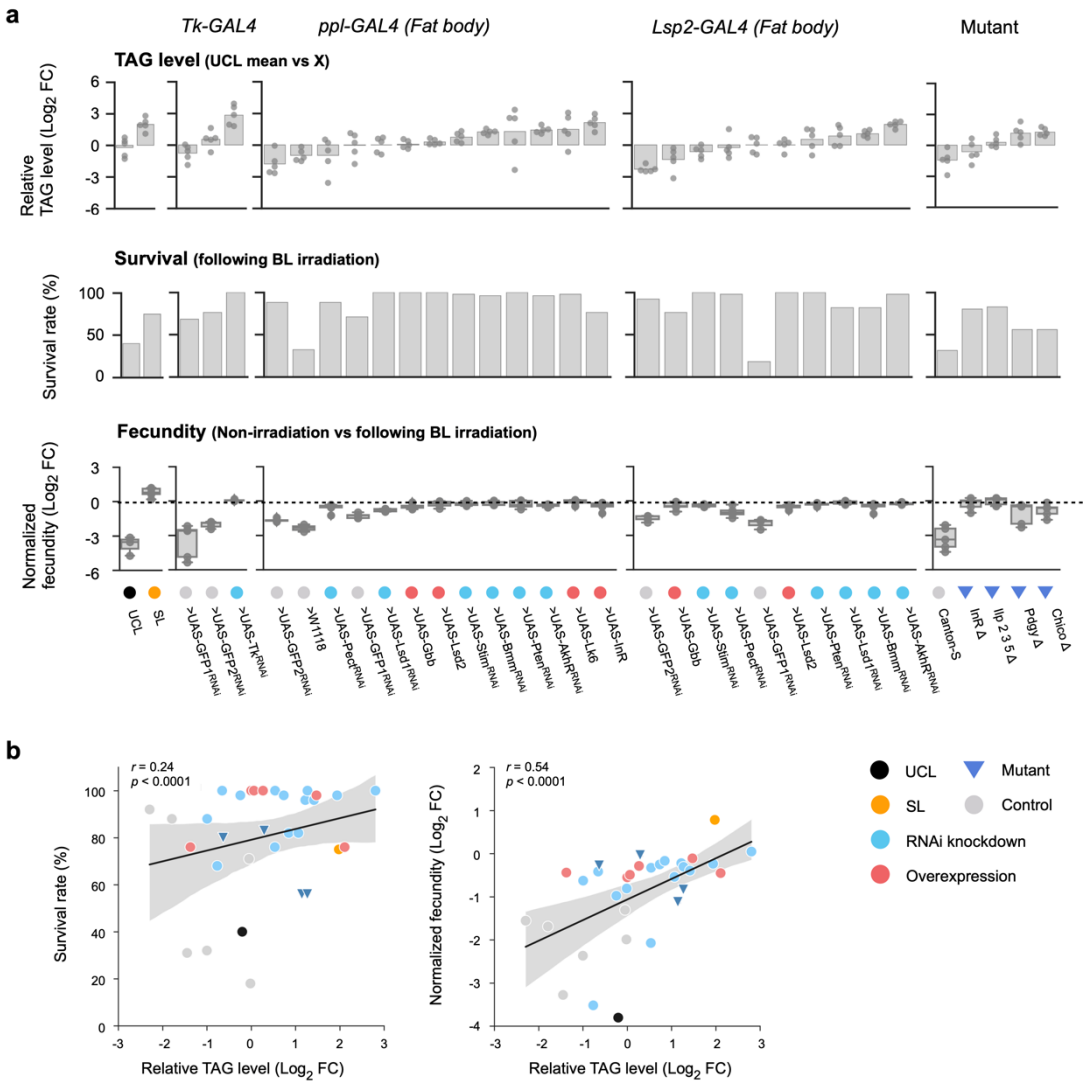

Fig. 5 | Lipid accumulation via genetic manipulation confers BL-tolerance

a, Top: Relative TAG levels. Middle: Survival rates following BL irradiation. Bottom: Normalized fecundity. **b**, Correlation analysis: Left - Survival rate with Relative TAG levels (r = 0.24, p < 0.0001). Right - Number of offspring with Relative TAG levels (r = 0.54, p < 0.0001). For details, see Supplementary Table 5 for all results, including target genes.

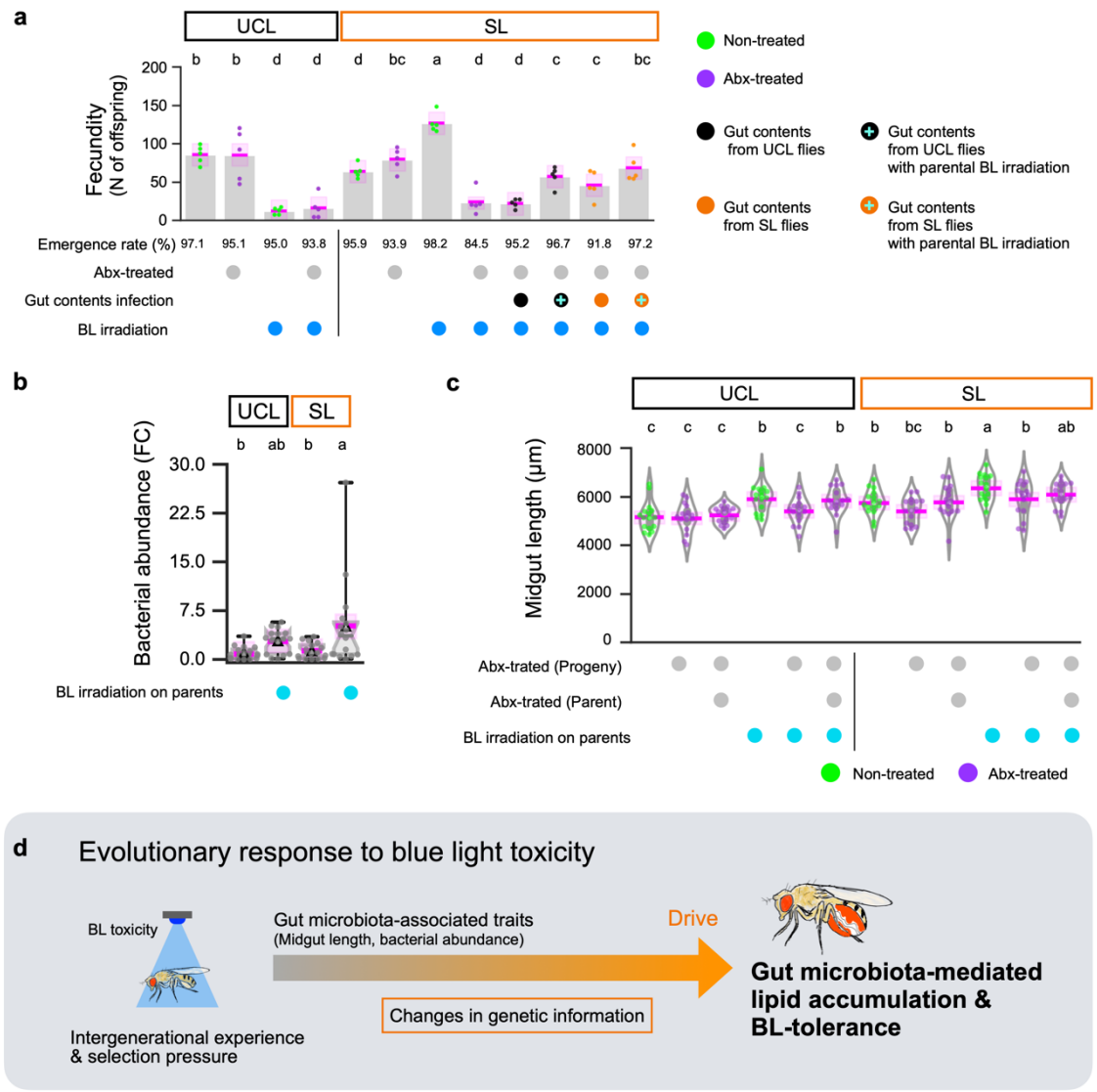

Fig. 6 | Parental experience of BL irradiation affects progeny's gut microbiota-associated traits

a, Fecundity; number of offspring (adults). n = 5. BF_{10} >100. (Replicate line 1, Generation 53). **b**, Bacterial abundance. n = 16. BF_{10} = 63.02. (Replicate line 1, Generation 53). **c**, Midgut length. n = 16, BF_{10} >100 (Replicate line 1, Generation 54). **d**, Evolutionary response to blue light toxicity. The selective pressure and the intergenerational repetition of parental experiences can alter genetic information, driving midgut elongation and increasing bacterial abundance. This process facilitates the formation of an adaptive physiological phenotype, characterized by lipid accumulation via the gut microbiota. Statistical analyses for panels **a**-

c were performed using HBM with MCMC methods, posterior median, and Bayesian 95% CI. Significant differences between different letters indicate *p*MCMC < 0.05. For details, see Supplementary Table 6 for all results, including statistical models.

1169 # Supplementary Figures

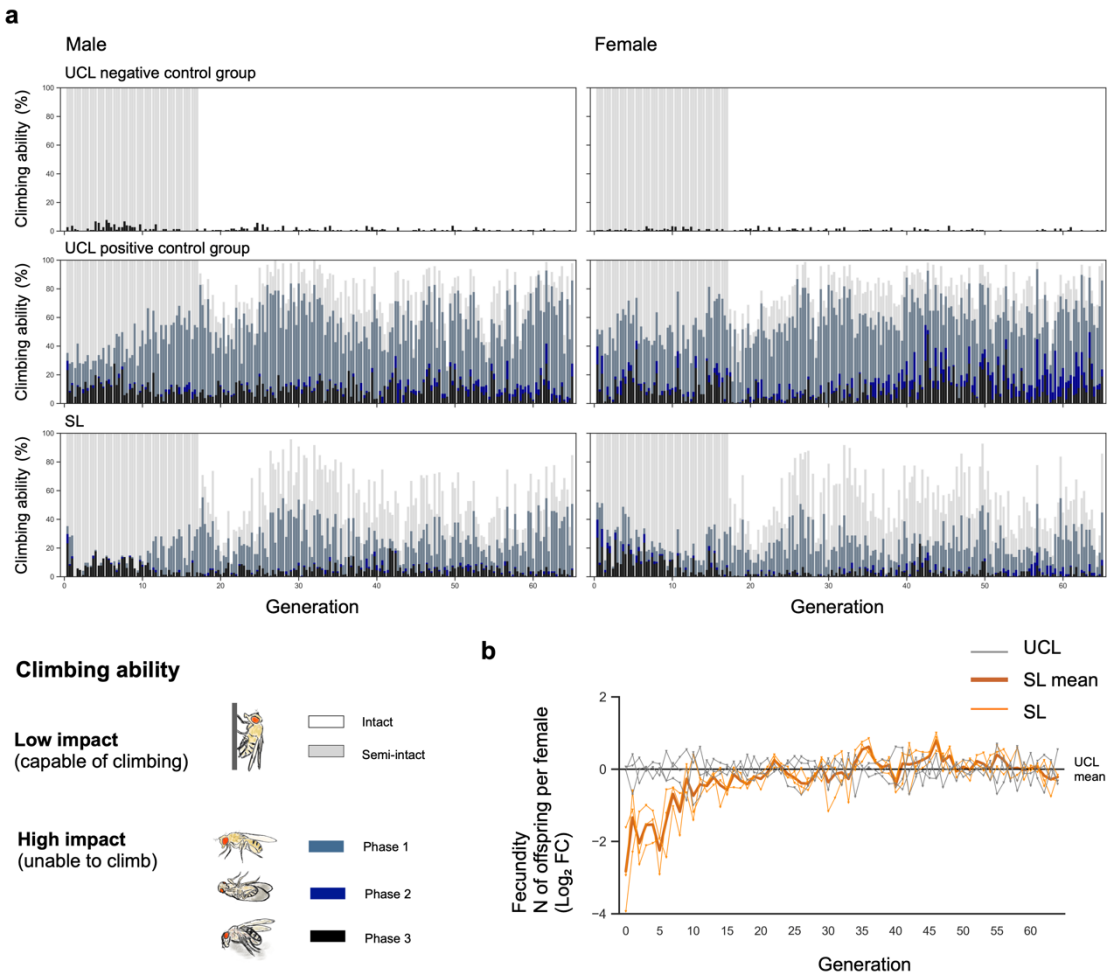

1170

1171 **Supplementary Fig. 1 | SL flies exhibit BL-tolerance**

1172 **a,** Climbing ability following BL irradiation and generational changes resulting from
1173 laboratory selection. Climbing ability is represented by a total of 60-100 flies per bar, with
1174 bars representing replicate lines 1, 2, and 3. Left: males, right: females The three
1175 categories are: Top - UCL non-irradiation (negative control group), Middle - UCL following
1176 BL irradiation (positive control group), and Bottom - SL following BL irradiation. **b,** Changes
1177 in fecundity across generations resulting from laboratory selection. The number of offspring
1178 per female (pupae) is shown. Data from Fig. 1d were Log_2-transformed relative to the
1179 average UCL value.

1180

1181

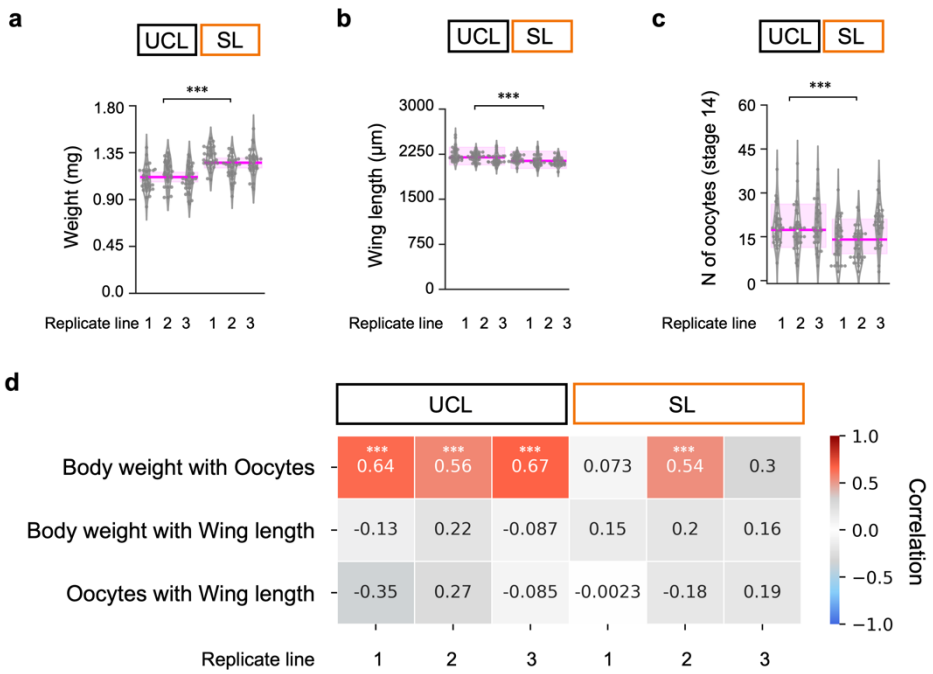

Supplementary Fig. 2 | SL flies are characterized by heavier body weight, shorter wing length, and a lower oocyte count

a, Body weight. n = 90, BF_{10} > 100 (Generation 28). **b**, Wing length. n = 90, BF_{10} = 91.1 Generation 28). **c**, Number of stage 14 oocytes. n = 90, BF_{10} = 2.46 (Generation 28). **d,** Correlation between traits, based on data from panels **a**-**c**. Asterisks indicate significance: *** p < 0.001.

Statistical analyses for panels a-c were performed using a HBM with MCMC methods, posterior median, and Bayesian 95% CI. Asterisks indicate significance levels: *** pMCMC < 0.001. For details, see Supplementary Table 7 for all results, including statistical models.

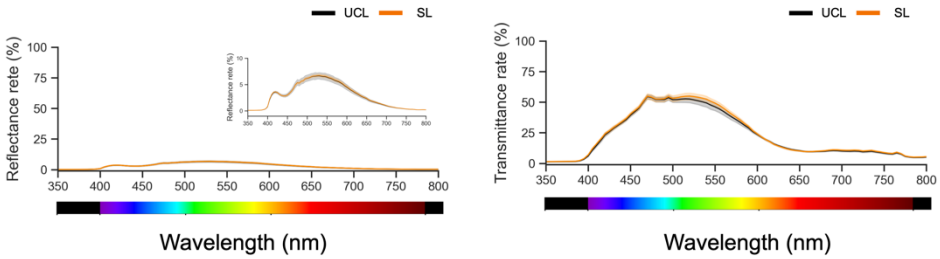

Supplementary Fig. 3 | SL flies show no physical differences in response to light

Reflectance rate and transmittance rate in female abdomen: left, reflectance rate; right, transmittance rate, *n* = 16 (Replicate line 1, Generation 49).

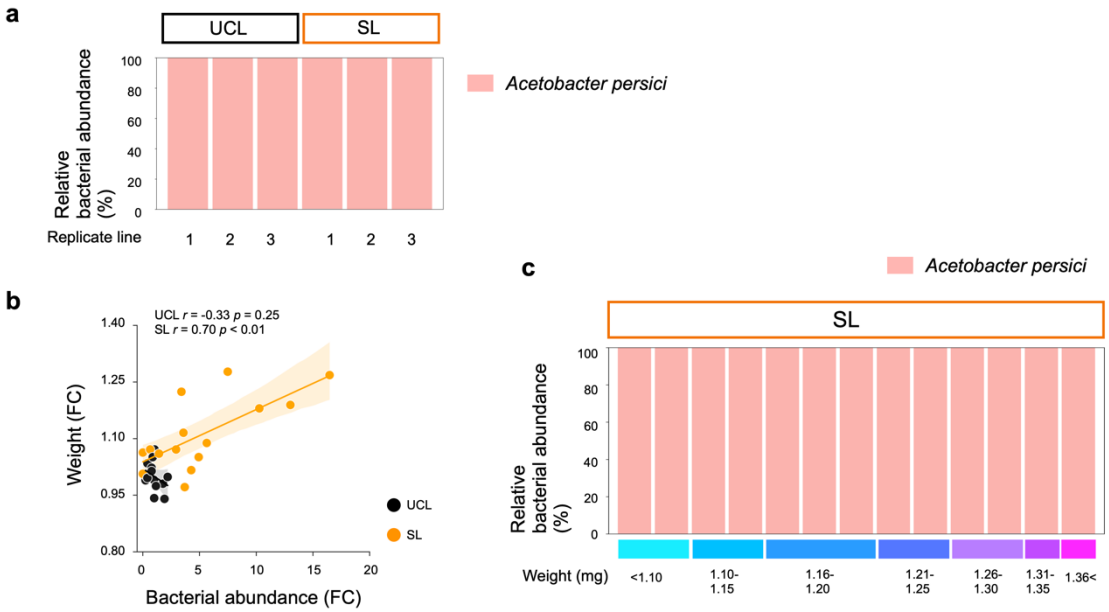

Supplementary Fig. 4 | The gut microbiota of SL flies consists of a single *Acetobacter* species, with bacterial abundance positively correlated with body weight

a, 16S/ITS rRNA amplicon sequencing results. The DNA samples used were the same as those employed for WGS in Fig.4 a (Generation 44). **b**, Correlation between body weight and bacterial abundance, based on data from panel Fig. 3a. Data for body weight and bacterial abundance were normalized to the mean UCL values from corresponding replicate lines. **c**, 16S/ITS rRNA amplicon sequencing results (SL Replicate line 1 Generation 45).

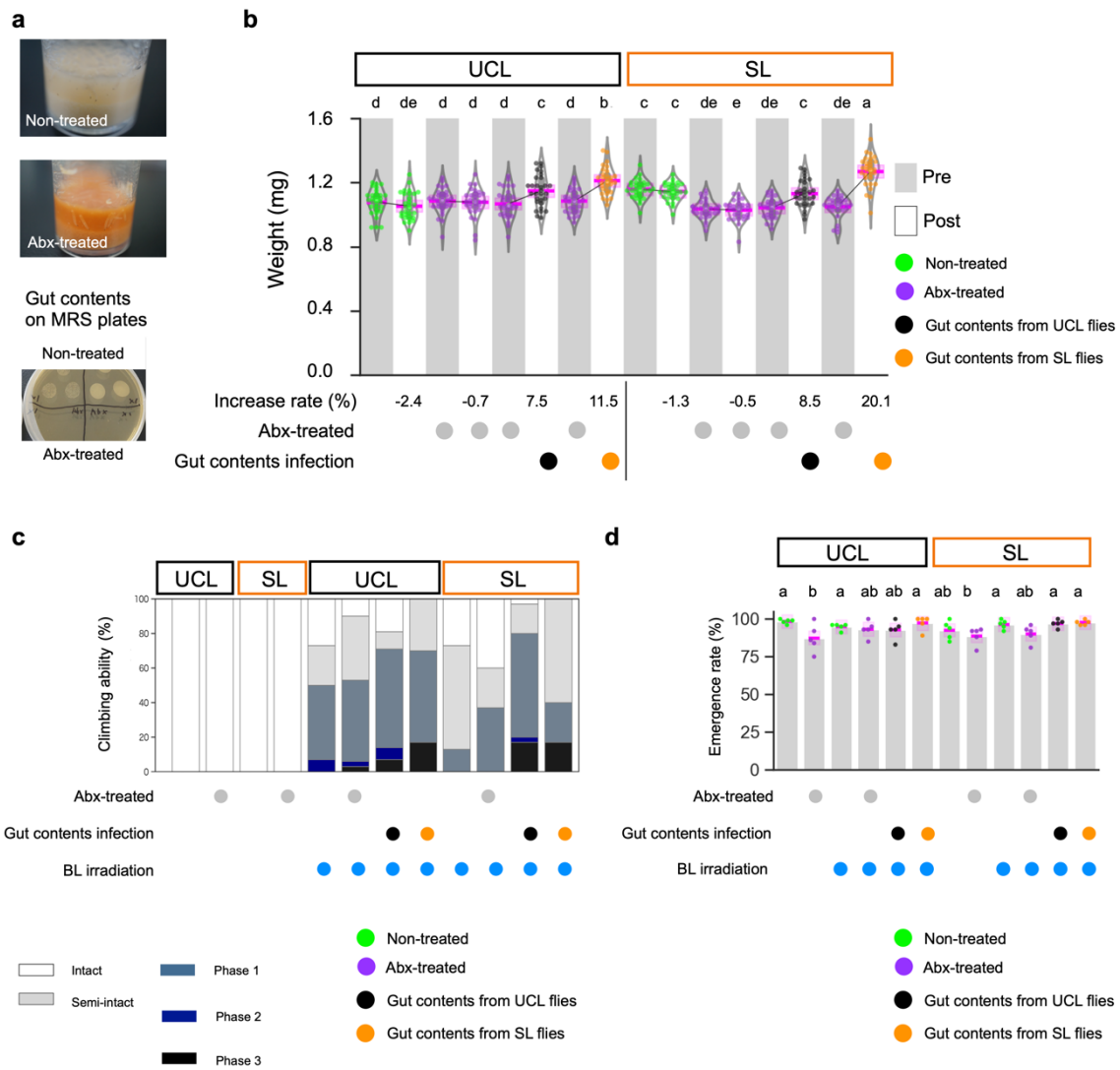

Supplementary Fig. 5 | The unique phenotypes of SL flies depend on gut microbiota

a, Effect of antibiotic mixture (Abx) treatment on gut microbiota. **b**, Impact of Abx treatment and gut contents infection on body weight. Grey bars represent pre-infection, while white bars indicate post-infection after 4 days. n = 30, BF_{10} > 100 (Replicate line 1, Generation 47). **c**, Climbing ability following BL irradiation. Climbing ability is represented by a total of 30 flies per bar (Replicate line 1, Generation 47). **d**, Emergence rate, based on data from Fig. 3d. BF_{10} = 1.30 (Replicate line 1, Generation 47).

Statistical analyses for panels **b** and **d** were performed using HBM with MCMC methods.

Significant differences between different letters indicate *p*MCMC < 0.05. For details, see Supplementary Table 8 for all results, including statistical models.

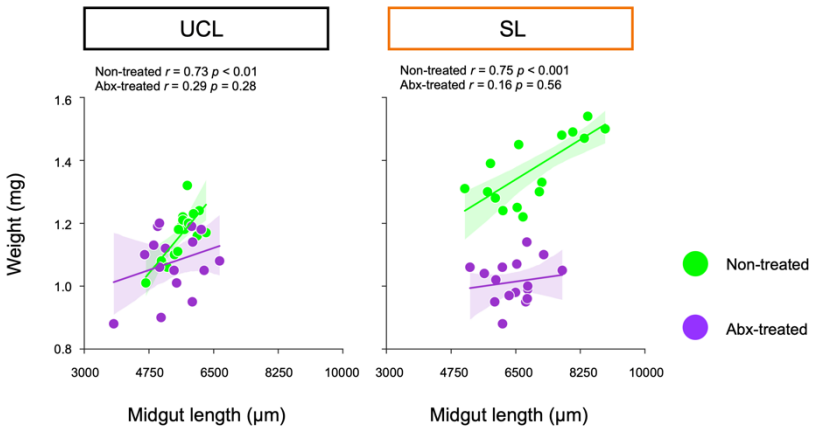

Supplementary Fig. 6 | A positive correlation between midgut length and body weight is observed under microbiota-present conditions

Correlation between body weight and midgut length, based on data from Fig. 3h.

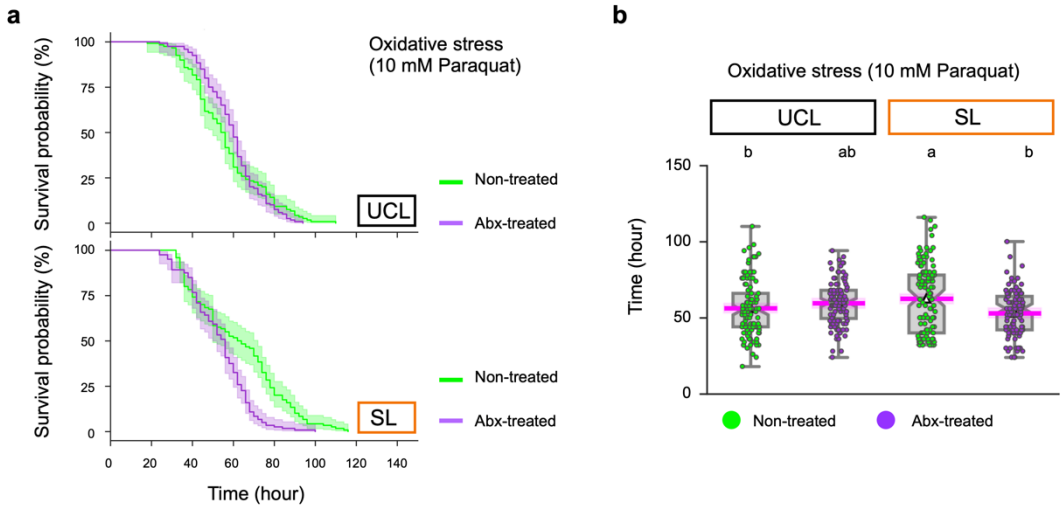

1228

1229 **Supplementary Fig. 7 | Oxidative stress resistance in SL flies is observed**

1230 **only in the presence of microbiota**

1231 **a**, Oxidative stress resistance in SL flies treated with 10 mM paraquat. Kaplan-Meier

1232 survival curve, *n* = 120 (Generation 52, Replicate line 1).

1233 **b**, Oxidative stress resistance in SL and UCL flies treated with 10 mM paraquat. *n* = 120,

1234 BF_{10} = 0.01. Survival: Estimates: non-treated UCL 56.36 h (53.29 to 59.43), Abx-treated

1235 UCL 59.57 h (56.33 to 62.61), non-treated SL 62.48 h (59.42 to 65.64), Abx-treated SL

1236 53.10 h (50.02 to 56.22). (Generation 52, Replicate line 1).

1237 Statistical analysis was performed using HBM with MCMC methods. Significant differences

1238 between different letters indicate *p*MCMC < 0.05. For details, see Supplementary Table 9 for

1239 all results, including statistical models.

1240

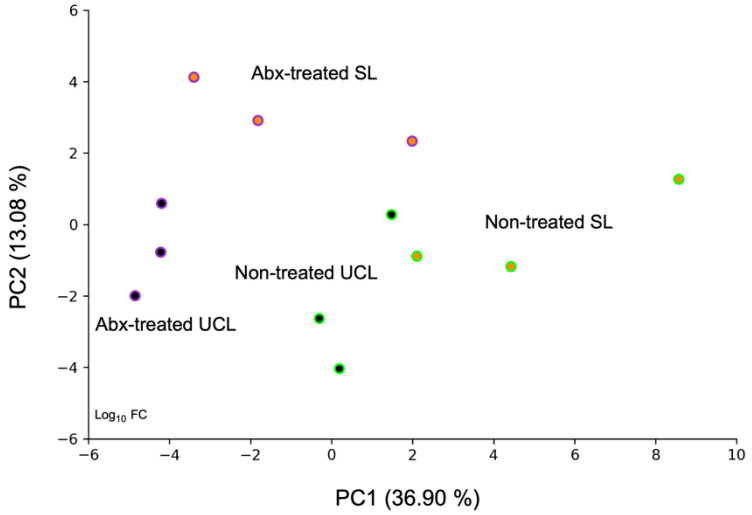

1241

1242 **Supplementary Fig. 8 | Characteristic transcriptome profiles of non-treated**

1243 **SL flies**

1244 Principal component analysis of transcriptome profiles from non-treated SL flies. Count data

1245 were standardized using Log_{10} fold change.

1246

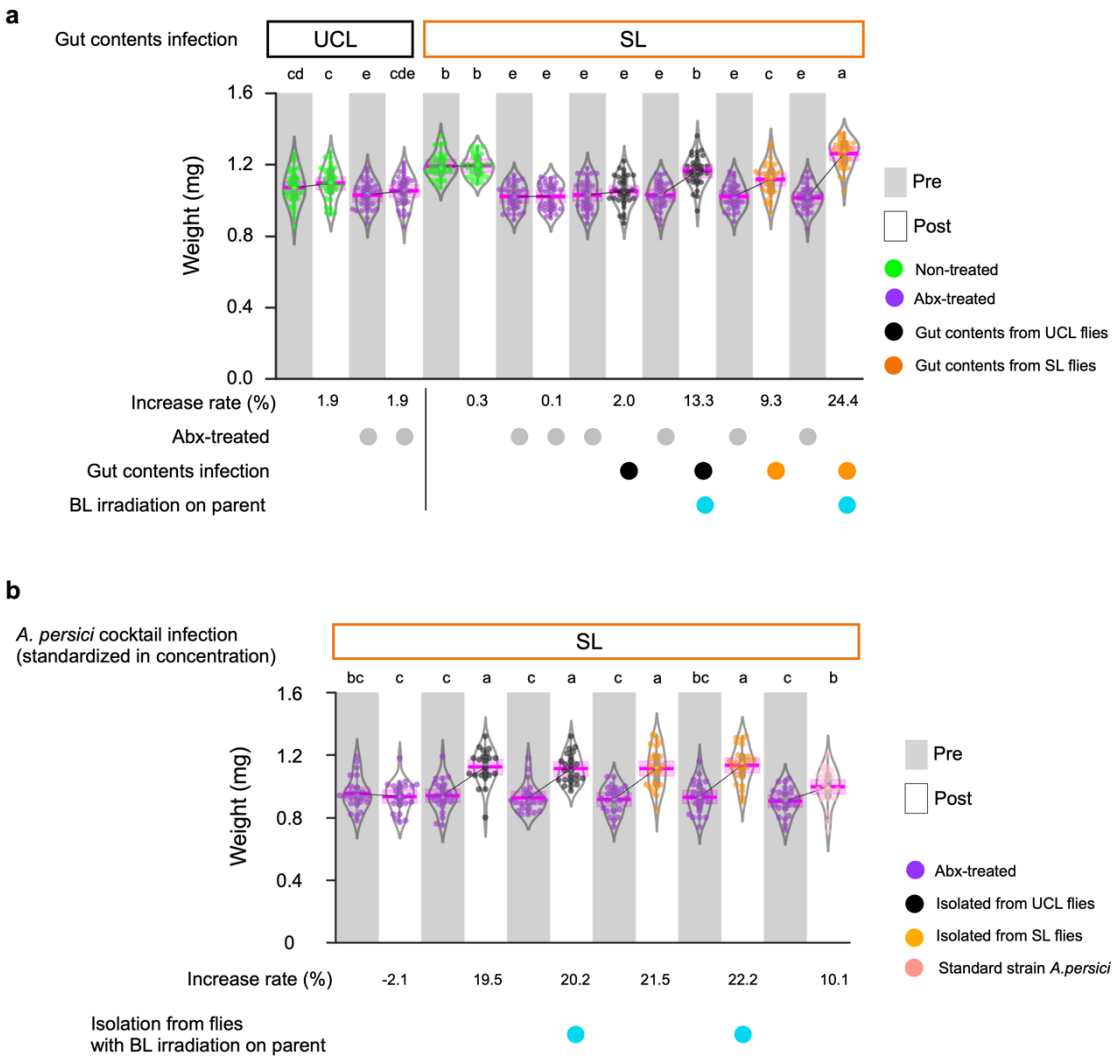

Supplementary Fig. 9 | Greater bacterial abundance leads to higher body weight

a, Impact of gut contents infection on body weight. Grey bars represent pre-infection, while white bars indicate post-infection after 4 days. n = 30, BF_{10} > 100 (Replicate line 1 Generation 53). **b**, Impact of *Acetobacter persici* cocktail infection on body weight. Grey bars represent pre-infection, while white bars indicate post-infection after 4 days. n = 30, BF_{10} >100 (Replicate line 1 Generation 53).

Statistical analyses for panels **b** and **d** were performed using HBM with MCMC methods. Significant differences between different letters indicate pMCMC < 0.05. For details, see

Supplementary Table 10 for all results, including statistical models.

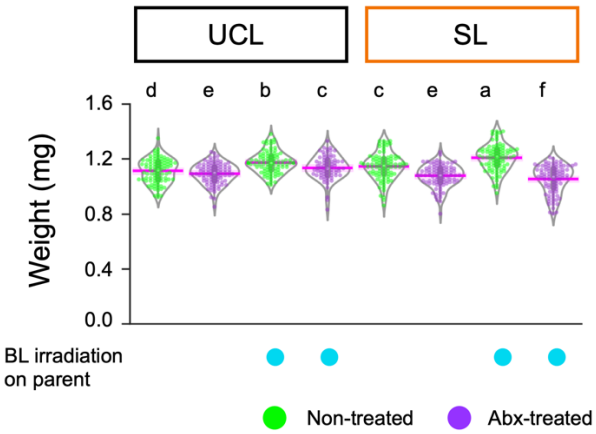

Supplementary Fig. 10 | Parental BL experiences induce increased progeny's body weight

Female body weight. *n* = 72-90, BF_{10} > 100. Statistical analysis was performed using HBM with MCMC methods. Significant differences between groups are indicated by different letters, with *p*MCMC < 0.05 (Replicate line 1, Generation 46). For details, see Supplementary Table 11 for all results, including statistical models.